

Land Surface-Convective Precipitation Feedbacks:

Theory and Application

by

Alexandra G. Konings

Department of Environment
Duke University

Date: _____

Approved:

Gabriel G. Katul, Supervisor

Amilcare Porporato

Sari A. Palmroth

Thesis submitted in partial fulfillment of the requirements for the degree of
Master of Science in the Department of Environment
in the Graduate School of Duke University
2011

ABSTRACT
(Hydrology)

Land Surface-Convective Precipitation Feedbacks: Theory
and Application

by

Alexandra G. Konings

Department of Environment
Duke University

Date: _____

Approved:

Gabriel G. Katul, Supervisor

Amilcare Porporato

Sari A. Palmroth

An abstract of a dissertation submitted in partial fulfillment of the requirements for
the degree of Master of Science in the Department of Environment
in the Graduate School of Duke University
2011

Copyright © 2011 by Alexandra G. Konings
All rights reserved except the rights granted by the
Creative Commons Attribution-Noncommercial Licence

Abstract

In this thesis, an intermediate-level complexity model of a coupled land-surface and atmospheric boundary layer is developed. The model is used to investigate the controls on soil moisture-precipitation feedbacks and vegetation biomass-precipitation feedbacks. The diurnal evolution of a well-mixed boundary layer with piece-wise linear profiles of potential temperature and specific humidity is modeled. Rainfall can (though is not guaranteed to) occur if the boundary layer height crosses the lifting condensation level and if the boundary layer height is sufficiently high relative to the Obukhov length. The model illustrates that precipitation occurrence is more sensitive to the free atmospheric humidity profile than to the free atmospheric temperature profile. The precipitation model is also coupled to a model of spatial vegetation patterns in the Sahel to investigate the timescales of vegetation pattern response to changes in rainfall regime. Land surface-precipitation feedbacks increase the sensitivity and rate of change of vegetation pattern morphology.

Contents

Abstract	iv
List of Tables	vii
List of Figures	viii
Acknowledgements	ix
1 Introduction	1
1.1 The need for an intermediate-level complexity model	3
1.2 Vegetation patterning and rainfall feedbacks	4
2 The Rainfall-no Rainfall Transition in a Coupled Land-Convective Atmosphere System	7
2.1 Introduction	7
2.2 Model description	8
2.2.1 Precipitation	12
2.3 Limiting Behavior	14
2.4 Dry air entrainment influence on surface partitioning	17
2.5 Conclusions	18
3 Spatial Patterns and Rainfall Feedbacks Determine Drought Sensitivity of Patterned Vegetation	19
3.1 Introduction	19
3.2 Methods	23
3.2.1 Conceptual framework	23

3.2.2	ABL model	25
3.2.3	Surface cover model	28
3.2.4	Model parameterization	33
3.2.5	Analysis	37
3.2.6	Experimental Design	37
3.2.7	Analysis Metrics	40
3.3	Results	42
3.3.1	Q1: How and how fast do modeled vegetation patterns respond to changes in rainfall regime?	42
3.3.2	Q2: How do the two types of vegetation-precipitation feedbacks affect the response?	44
3.4	Discussion and Conclusions	50
4	Conclusions	54
4.1	Summary of Results	54
4.2	Future Work	56
4.2.1	Rainfall Model	56
4.2.2	Patterned vegetation	58
4.3	Broader implications	61
A	Model equations	63
A.1	Soil moisture	63
A.2	Surface energy partitioning	64
A.3	Atmospheric boundary layer growth	66
A.4	Rainfall depth	66
	Bibliography	68

List of Tables

3.1	Treatment of precipitation feedbacks and dynamics in some patterned vegetation studies	22
3.2	Parameter values used in surface cover model	34

List of Figures

2.1	Summary of the modeled triggering process.	9
2.2	Histograms of free atmospheric parameters measured at two different locations	11
2.3	Relationship between ϕ_q and early-morning relative humidity	12
2.4	Relationship between the slope and intercept of the free atmospheric humidity profile	13
2.5	Stationary state space as a function of FA parameters	14
2.6	Effect of dry-air entrainment on EF sensitivity to soil moisture	16
3.1	Spatial and temporal scales of several processes impacting vegetation patterns	25
3.2	Seasonal cycle of measured free atmospheric parameters	36
3.3	Key pathways of model influence of vegetation biomass on rainfall	39
3.4	Entropy variation with pattern type	42
3.5	Pattern morphology evolution during drought	43
3.6	System evolution during droughts of different magnitudes	44
3.7	Rainfall statistics for different feedback scenarios	48
3.8	System evolution during drought for different feedback scenarios	49

Acknowledgements

My research has been generously supported by the National Science Foundation Graduate Research Fellowship Program and by a James B. Duke fellowship.

Gaby Katul has been a wonderful advisor. His honest concern about my academic, professional, and personal evolution was clear in all he did. Despite a busy to-do list, he has always been willing to put other work aside to help me. I am very grateful for all his advice and support throughout my M.S. career - from the days when I was deciding to come to Duke to all the plans we have made for further work. I am grateful to Stefan Dekker of Utrecht University, my collaborator on the project on which Chapter 3 of this thesis is based, for his insightful questions and suggestions. Amilcare Porporato was very helpful as a collaborator on the work of Chapter 2, and as a general mentor over the course of the last two years. Sari Palmroth was willing to be on my committee at the last minute. I thank her for working so hard to fulfill this role even if it required catching up on my work in only a short period of time.

Lastly, thanks are due to the members of the Katul lab for many discussions - from insightful to relaxing, and from brief to long; many thanks to Kim Novick, Sally Thompson, and Dani Way. Thanks also to Stefano Manzoni, Annalisa Molini, and Giulia Vico.

1

Introduction

Climate had traditionally been considered as a set of fixed forcing parameters influencing land surface processes. In the 1970's and 1980's, awareness grew that many land surface processes may in turn affect climate [*Eagleson*, 1970; *Charney*, 1975; *Shukla and Mintz*, 1982], creating a feedback. Since then, so-called 'land-atmosphere interactions' have received much research attention [see partial reviews in *Entekhabi*, 1995; *Pitman*, 2003]. Much of this attention, including several major field campaigns [*Sellers et al.*, 1992; *Andre et al.*, 1986], has focused on accounting for land-atmosphere interactions in climate models. It can be difficult to disentangle the effects of such interactions, or feedbacks, from background environmental variability, particularly if more than two variables are coupled. Furthermore, systems with strong positive feedbacks often show enhanced sensitivity to small changes, leaving the system open to 'regime shifts', or fundamental changes in behavior. Understanding and predicting the system behavior may therefore be considerably be more difficult if feedbacks are present.

The focus of this thesis is on feedbacks between the land surface and convective precipitation occurrence. The impact of the land surface on convective precipitation

is among the most challenging problems in land atmosphere interactions. Climate change is expected to increase the frequency and intensity of droughts [*Easterling et al.*, 2000], with resulting changes in ecosystem and agricultural productivity, and perhaps even vegetation die-off [*Breshaers et al.*, 2005]. Land surface-precipitation feedbacks may exacerbate the effects of these droughts. Additionally, large-scale management decisions may need to account for the effect of potential land cover change on precipitation and area water resources. Previous work has already suggested historical land cover change affected climate [*Baidya Roy et al.*, 2003a; *Jackson et al.*, 2005].

Among the many components that contribute to the land surface state, this thesis focuses on soil moisture and vegetation cover. Feedback pathways exist not only between both of these variables and convective precipitation, but also between the variables themselves. For example, increased soil moisture may support higher vegetation growth, which increases transpiration and reduce soil moisture. Both vegetation cover and soil moisture may change albedo, while changes in albedo change the energy balance of the surface, in turn affecting soil moisture (through changes in evapotranspiration) and vegetation development (through changes in evapotranspiration and temperature).

Soil moisture may also mediate the effect of groundwater on precipitation. Catchment model studies indicate variable groundwater depth contributes to the land surface-precipitation feedback strength [*Ferguson and Maxwell*, 2010]. *Bierkens and van den Hurk* [2007] also argue that in areas with appropriate topography, convergence of groundwater in low lying areas allows groundwater to directly influence surface fluxes, and enhances the land surface-precipitation feedbacks on multi-year timescales. However, the effect of groundwater variability on precipitation is beyond the scope of this thesis.

1.1 The need for an intermediate-level complexity model

Within the hydrologic community, much research on soil moisture-precipitation feedbacks has focused on determining where surface feedbacks have the greatest effect on improving seasonal-scale precipitation predictions of global circulation models (GCMs), [e.g. *Koster et al.*, 2006]. However, GCMs may not accurately represent the coupling between land and atmosphere, as can be seen not only by comparing model results to surface measurements across a wide variety of locations [*Dirmeyer et al.*, 2006], but also through the significant variability in feedback predictions of different GCMs [*Guo et al.*, 2006]. Most research on vegetation cover-precipitation feedbacks has focused on the potential consequence of Amazonian deforestation [*Baidya Roy and Avissar*, 2002; *Wang et al.*, 2009], which is likely influenced by the spatial scales and patterns at which deforestation occurs [*Baidya Roy et al.*, 2003b]. Effects of large-scale deforestation in the Amazon may influence not only local precipitation, but also induce precipitation changes in other areas of the globe [*Werth and Avissar*, 2002]. Studies of the effects of deforestation and agricultural conversion in countless other regions exist.

Despite such considerable research attention on land surface-precipitation feedbacks, a clear picture of what determines feedback strength and how to ‘fingerprint’ its onset has not yet emerged. Numerous different physical mechanisms (pathways) exist that cause coupling between land surface moisture and cover [*Santanello et al.*, 2007; *van Heerwaarden et al.*, 2009]. The relative sizes of each of the pathways varies regionally and temporally. As a result, it is difficult to predict *a priori* how much each pathway will contribute to the total feedback, if at all. It is theoretically possible to determine the relative strength of different pathways, and thus of the total feedback, based on statistical analysis of land surface and atmospheric variables. However, the strong non-Gaussian distribution of precipitation and other variables and the lack

of a clear timescale associated with many processes make it difficult to establish a strong statistical signal. This problem is aggravated by the limited length of many datasets. As a result, determining feedback strength purely from data remains an unpopular, though perhaps underutilized, approach.

This thesis explores some of the factors controlling precipitation feedbacks by using models of only the minimum necessary complexity. The reduced complexity (relative to many established models) allows for a more tractable analysis of system behavior, and therefore allows for a greater understanding of the physical processes. The basic model, described in Chapter 2, is based on the hypothesis that even when land surface conditions appear to regulate feedback strength, it is possible to identify a set of forcings derived from atmospheric dynamics that control the onset of this feedback. Although the precipitation model used is not sufficiently complex to predict whether or not feedbacks actually occur (that is, it provides ‘necessary but not sufficient’ conditions), it is still able to show when feedbacks are not possible. In Chapter 2, the implications of this model’s behavior for the relative importance of atmospheric humidity and atmospheric temperature profiles are analyzed. Aside from providing general scientific insight, the model can also be applied to specific regions. In Chapter 3, this is done for semi-arid ecosystems in Southwestern Niger that exhibit spatial vegetation patterns.

1.2 Vegetation patterning and rainfall feedbacks

The West African Sahel includes some of the world’s poorest countries, where water resources and other environmental factors strongly limit agricultural productivity. A drought has plagued the region for the last half century, and is expected to continue through the next century [*Held et al.*, 2005]. Anthropogenic land use forcings are generally believed to have contributed to (though not been the sole cause of) this drought [*Zeng*, 2003].

The existence of regular spatial patterns in semi-arid vegetation structure was first noticed in aerial photographs in the 1950's [e.g. *MacFadyen*, 1950], and has also been found in many sites in the Sahel [*Leprun*, 1999; *Valentin and d'Herbes*, 1999; *Barbier et al.*, 2006]. Over the last decade, theoretical studies investigating these patterns have promoted their potential use as indicators of system nearness to desertification [*Rietkerk et al.*, 2004; *Kefi et al.*, 2007]. Theoretical results further suggest that spatial vegetation patterning is indicative of hysteretic bistable systems in which the onset of desertification may be irreversible [*Rietkerk et al.*, 2004]. Although a variety of vegetation pattern models exist [*Rietkerk et al.*, 2002; *Lefever et al.*, 2009; *Gilad et al.*, 2007; *Borgogno et al.*, 2009], all models generally agree that vegetation patch formation is fundamentally a Turing-type process. That is, processes that promote pattern growth (i.e. increased infiltration capacity or through extension of root organs beyond the canopy patch) are opposed by other factors tending to suppress pattern growth (i.e. limited system-wide water resources). The number of field studies of vegetation pattern work has begun to increase, and remotely sensed images have been successfully used for vegetation patterning studies [*Deblauwe et al.*, 2008; *Barbier et al.*, 2006], demonstrating their potential for use in wide-spread monitoring efforts. However, no theoretical basis exists to study how transient behavior and forcing variability may affect inferences drawn from patterns. The temporal evolution of the desertification process have not been extensively considered.

Because vegetation patterns occur due to limitations in water resources, temporal variability in rainfall and vegetation-precipitation feedbacks are expected to significantly affect the dynamics of desertification in patterned systems. Land surface-precipitation feedbacks have been shown to be significant in the Sahel [e.g. *Zeng et al.*, 1999; *Wang and Eltahir*, 2000a,b], although there has been some disagreement about the predominant sign of the feedback in the region [*Taylor and Ellis*, 2006; *van den Hurk and van Meijgaard*, 2010]. Climate models used to study

land-atmosphere interactions generally have too low a spatial resolution to resolve vegetation spatial patterns, and cannot account for the sub-grid scale soil moisture variability that allows vegetation patterns to persist. On the other hand, models of vegetation patterns have generally considered rainfall as a fixed input parameter, and have not considered feedbacks. Because of its relative simplicity, the intermediate-level model of precipitation developed in Chapter 2 provides a means to explicitly resolve both vegetation patterns and precipitation feedbacks in a single model. In Chapter 3 of this thesis, the model is coupled to a model of spatial vegetation patterns. The resulting simulation system is used to predict the timescales associated with vegetation pattern change occurring due to shifts in the rainfall regime. Aside from providing preliminary insight into whether these ecosystems are likely to collapse during specific droughts, comparing the timescales (once verified in the field) to those of observed vegetation pattern change may assist in determining whether other ecosystem stressors are present. The significant effect precipitation feedbacks have on the predicted timescales illustrates the importance of understanding the behavior of surface-precipitation interactions.

The Rainfall-no Rainfall Transition in a Coupled Land-Convective Atmosphere System

2.1 Introduction

If atmospheric conditions are favorable, the soil moisture state may affect the disposition to and occurrence of convective rainfall [Ek and Holtslag, 2004; Findell and Eltahir, 2003]. Since soil moisture depends on rainfall occurrence, rainfall represents a feedback pathway in the coupled soil-plant-atmosphere system. This ‘soil-moisture precipitation feedback’ has received significant research attention given its role in the climate system. The physical mechanisms of this feedback are complicated by a large number of interacting processes occurring between the land surface and the atmospheric boundary layer (ABL) state. Juang *et al.* [2007] analyzed two ‘necessary but not sufficient’ conditions for rainfall to occur: (i) the crossing of the boundary layer height (h) and the lifting condensation level (LCL), and (ii) an atmosphere that supports the continuation of convection once it is initiated. With regards to the first necessary condition, surface processes and free atmospheric (FA) temperature and humidity profiles affect both ABL growth and LCL evolution, and often in coun-

teractive ways. For example, a large surface heating and a low evaporative fraction (EF, the ratio of evapotranspiration to available energy) leads to increased boundary layer growth, entrainment of dry air and subsequent decrease in atmospheric humidity. The decrease in atmospheric humidity leads to an increased driving force for evaporation, resulting in a decrease in surface heat flux at later times. This pathway is referred to here as the dry-air entrainment feedback [*Santanello et al.*, 2007; *van Heerwaarden et al.*, 2009]. The initial increase in h promotes a crossing of the ABL and LCL; however, the subsequent reduction in atmospheric humidity elevates the LCL, making a crossing less likely.

Given such simultaneous effects of surface and FA conditions on ABL and LCL dynamics, it is not surprising that much of the existing literature on the soil-moisture precipitation feedback generally falls into one of two categories: either the focus is on the effect of the land surface state under prescribed FA conditions tied to particular geographic locations (e.g. [*Koster et al.*, 2006]), or the effect of FA profiles on ABL and LCL dynamics given a land surface state (e.g. [*Wu et al.*, 2009]). The main objective here is to assess the relative importance of FA and surface conditions on the ABL’s ability to support convective rainfall when both interact through the ABL. To do so, one must account not only for the auto-correlative properties of the FA parameters, but also the behavior of wind speeds and non-convective rain. Such an analysis would be prohibitively complex, preventing a clear theoretical treatment. Instead, this work explores the dynamics of an idealized coupled land surface-ABL system. Model results illustrate the preferential behavior of this coupled system, and clarify the role of land surface feedbacks.

2.2 Model description

A fully mixed ABL with potential temperature θ and specific humidity q constant throughout is assumed. The capping inversion at the top of the ABL is represented

by an instantaneous jump in both variables. Such zeroth-order jump models are shown to be effective at describing primarily the evolution of the boundary layer states [Pino *et al.*, 2006]. Warm, dry air is entrained at the inversion. Heat and moisture are added to the boundary layer at the surface, as determined by a surface energy partitioning model that accounts for the effects of both the soil and ABL states. Here, convection can be triggered only when the ABL height and the LCL cross. When rainfall occurs, its depth depends on the atmospheric humidity profile. Figure 2.1 summarizes these modeled processes. The Appendix also summarizes the model equations and parameters.

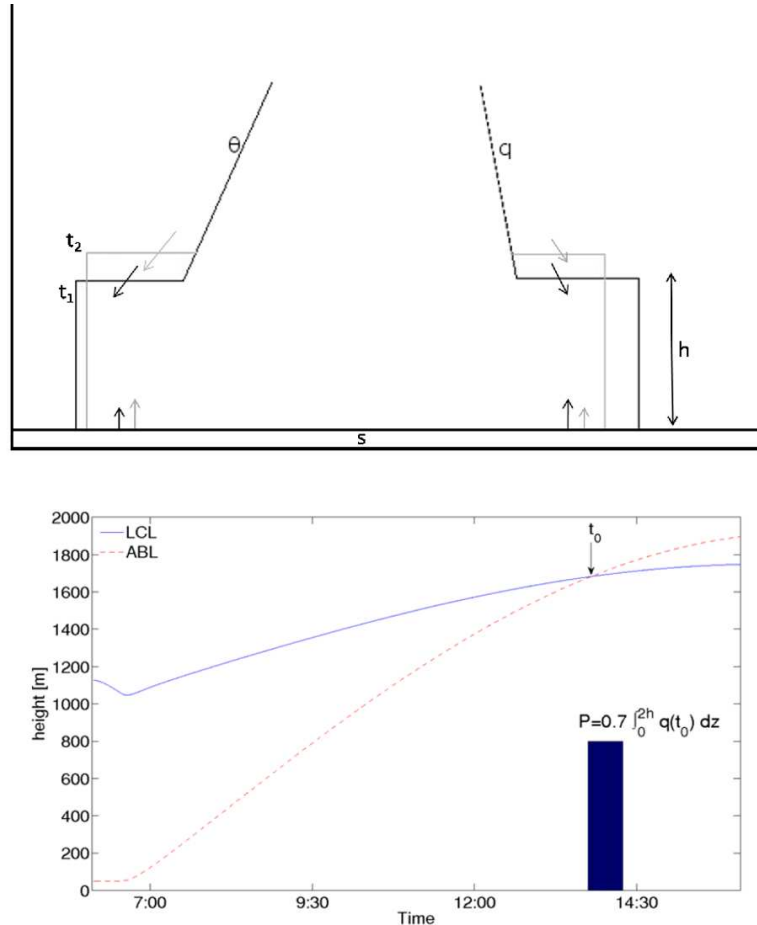


FIGURE 2.1: Summary of the modeled triggering process.

Heat and moisture fluxes at the surface are determined using an energy balance

combined with the Penman-Monteith equation for evapotranspiration. Within the energy balance, net radiation R_n is determined using astronomical equations for shortwave radiation and the ground heat flux is assumed to be 15% of this R_n . Although the exact value of incoming radiation depends on latitude and time-of-year, these factors are not explicitly considered here. Instead, we scale R_n by a factor R_n^{\max} . The stomatal conductance g_s used in the Penman-Monteith equation is modeled according to a multiplicative Jarvis model, i.e. using stress functions of several factors to modify the maximum stomatal conductance g_{\max} . The g_s depends hyperbolically on the incident sunlight S (here proportional to R_n) [Lhomme, 2001]. It is also affected logarithmically by the vapor pressure deficit VPD [Oren *et al.*, 1999] and quadratically by θ [Lhomme, 2001]. Lastly, g_s depends on soil moisture s . If s is above a critical value s^* , $g_s = g_{\max}$, but g_s decreases linearly with s if below that value. If s is below the wilting point s_w , no evapotranspiration is possible [Daly *et al.*, 2004].

The soil moisture in the root zone of depth Z_r is evolved using a simple bucket model. Drainage is given by a Darcian flux, assuming a unit gradient. Only a loamy soil is considered. The qualitative results in Section 2.3 do not change for different soil types. Soil moisture is the only variable in the model with explicit day-to-day memory.

The growth rate of the ABL is modeled using common 1-D energy balance considerations as in Porporato [2009] so that it is proportional to the surface heat flux $\overline{\theta' \omega'_s}$ and inversely proportional to γ_θ , the lapse rate above the boundary layer. Since convective rainfall generally does not occur at night, the evening collapse of the ABL is not explicitly considered. Instead, h is re-initialized to 50 m every morning.

The FA θ and q profiles are modeled linearly with height z above the surface with slope γ and intercept ϕ , such that $\theta_o(z) = \gamma_\theta z + \phi_\theta$ and $q_o = \gamma_q z + \phi_q$. Simple conservation equations can then be used to determine the evolution of the mixed

layer temperature and humidity.

Daily early-morning sounding data from Greensboro, NC and Topeka, KS are used to estimate plausible FA profiles. The data set covers 36 years from May to September, when convective rainfall is most common. The lapse rate and intercept for both θ and q were estimated using a linear regression analysis applied between $z \in [300, 5000]$ m. The distribution of the resulting parameters is shown in Figure 2.2.

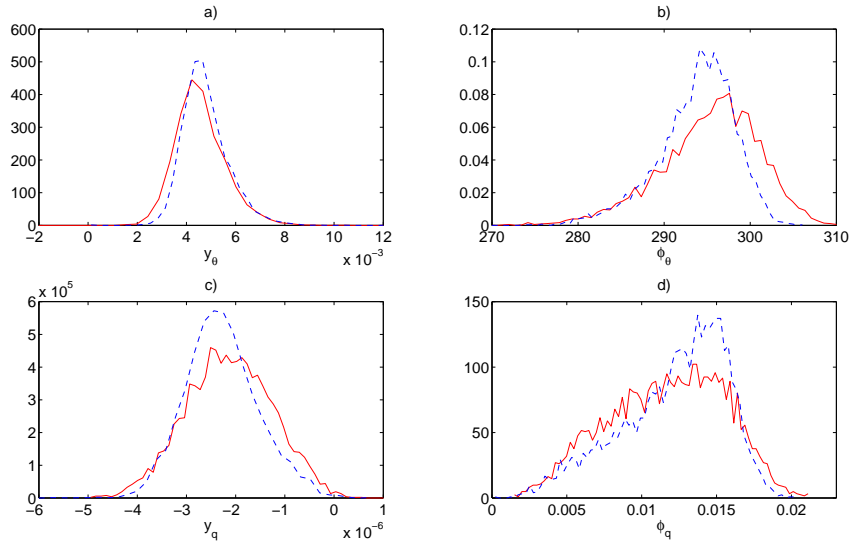


FIGURE 2.2: Histograms of the free atmospheric potential temperature and humidity parameters at Greensboro, NC (blue dashed line) and Topeka, KS (red line). a) Slope of potential temperature profile, b) Intercept of potential temperature profile, c) Slope of specific humidity profile, and d) Intercept of specific humidity profile. Profiles are calculated using a least-squares fit over 35 years of daily early-morning sounding data, for height $z \in [300, 5000]$ m.

Modelled θ and q are initialized every morning based on the profile intercepts. Early morning values depend on the residual layer remaining from the previous day’s collapsed ABL. Since FA properties have finite autocorrelation, a relationship between early morning θ and q and their daily free atmospheric profiles is reasonable. As shown in Figure 2.3 The equivalence assumed is supported when

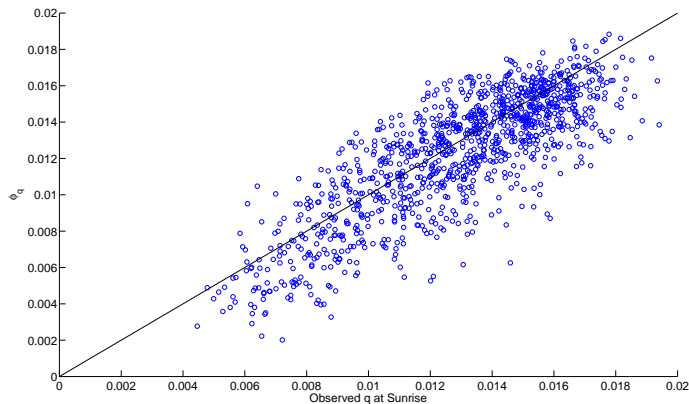


FIGURE 2.3: Relationship between the intercept of the daily free atmospheric humidity profile ϕ_q at Greensboro, NC and eddy-covariance measurements of humidity at sunrise 79 miles away near Durham, NC. The data cover the period from 1998 to 2005.

comparing Greensboro sounding data with θ and q measurements taken at sunrise with an eddy-covariance tower 79 kilometers away at the Duke Forest near Durham, NC, described by *Juang et al.* [2007]. Sounding data from both sites also support a negative linear relation between daily γ_q and ϕ_q , as shown in Figure 2.4. To reduce dimensionality, a similar relationship is adopted here. Although the exact relationship varies by location, qualitative results are not affected. In this case, $\gamma_q = -2.5 \times 10^{-4}\phi_q + 4 \times 10^{-7}m^{-1}$. Since the absolute value of the ABL θ (as influenced by ϕ_θ) has a far smaller effect than the absolute humidity, ϕ_θ is assumed constant at 294 K.

2.2.1 Precipitation

Modeling the initiation and sustaining of convection is quite complex and well beyond the scope here. One possible simplification is requiring $-z/L > 5$, where L is the Obukhov length based on land-surface fluxes of momentum, heat and water vapor, and $z = h/2$. This atmospheric stability threshold of 5 was chosen because buoyant production of turbulent kinetic energy becomes dominant within the ABL [*Kader*

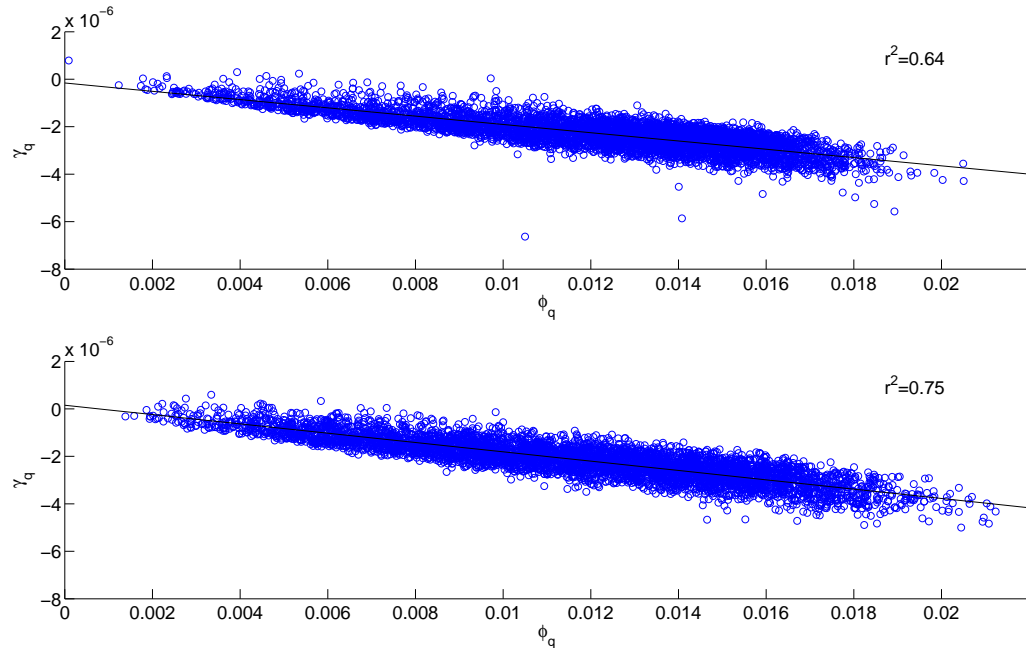


FIGURE 2.4: Scatter plot of daily free atmospheric humidity profile slope γ_q versus humidity profile intercept ϕ_q at Greensboro, NC (top) and Topeka, KS (bottom).

and Yaglom, 1990], thereby ensuring the generation of convection with sufficient buoyant plume velocity to reach the level of free convection. Juang *et al.* [2007] used half-hourly eddy-covariance measurements and a boundary layer model to predict when these two conditions were met above a forested system near Durham, NC. They showed that these conditions can be used effectively to predict the timing of convective rainfall when it occurs. The same framework is used here.

Since advection of water vapor is neglected, rainfall depth is taken to depend only on columnar water vapor [Muller *et al.*, 2009]. To prevent undue sensitivity to the height of the humidity profile, this column is ‘capped’ at $2h$. The total water vapor is multiplied by a precipitation efficiency equal to 0.7 [Brubaker and Entekhabi, 1995]. The results in section 2.3 are not sensitive to the exact rainfall scheme used (except for very small depths, $<1\text{-}2$ mm). The soil moisture-rainfall feedback is primarily dependent on the occurrence of rainfall rather than its depth, in agreement with the

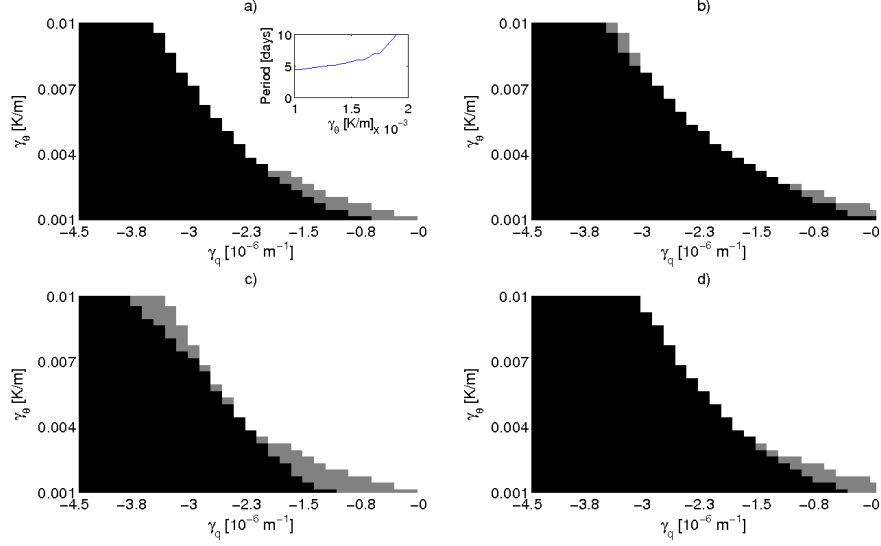


FIGURE 2.5: Stationary state space as a function of FA temperature and humidity profiles. Black indicates limit cycle with daily rainfall, gray indicates a limit cycle with a period greater than one day, and white areas do not rain. Each subplot represents a combination of daily R_n^{max} and g_{max} : a) $R_n^{max} = 350 \text{ W m}^{-2}$ and $g_{max} = 0.008 \text{ m s}^{-1}$, b) $R_n^{max} = 600 \text{ W m}^{-2}$ and $g_{max} = 0.008 \text{ m s}^{-1}$, c) $R_n^{max} = 350 \text{ W m}^{-2}$ and $g_{max} = 0.0016 \text{ m s}^{-1}$, and d) $R_n^{max} = 600 \text{ W m}^{-2}$ and $g_{max} = 0.0016 \text{ m s}^{-1}$. The inset shows the period of the limit cycle as a function of γ_θ in K m^{-1} for $\gamma_q = -1 \times 10^{-6} \text{ m}^{-1}$.

results of *D’Odorico and Porporato* [2004].

2.3 Limiting Behavior

To explore the limiting behavior of the model, we invoke two idealized assumptions: FA parameters are constant from day to day and precipitation always occurs when the triggering conditions are met. Depending on the combination of FA temperature and humidity profiles, the resulting stationary state for this simplified system is one of: rain storms occurring every day with oscillatory soil moisture behavior, a limit cycle in which rain storms occur every few days, or a permanent lack of rainfall. The final rainy/non-rainy state partly depends on the initial conditions for some combinations of FA parameters. The system evolves to the same stationary state independent of initial conditions when the initial $s > s^*$.

The distribution of limiting behaviors is shown in Figure 2.5 for combinations of the maximum net radiation and of g_{\max} . As γ_{θ} decreases and h grows faster, rain is possible over a wider range of humidity conditions. For a given temperature profile, rain only occurs if ϕ_q is sufficiently high (or, due to the relationship between ϕ_q and γ_q used here, if γ_q is sufficiently low) so that the LCL is sufficiently low for a crossing. Based on Figure 2.5, the atmosphere’s ability to support convective rainfall is more sensitive to the FA humidity profile than to the temperature profile. The former plays a stronger inhibitive role - when conditions are sufficiently dry, even the most unstable free atmospheres cannot support convection. Even for very stable free atmospheres, however, a sufficiently wet boundary layer still leads to triggering. Note that because of our assumption relating the early-morning humidity to ϕ_q and ϕ_q to γ_q , the sensitivity to γ_q shown in Figure 2.5 also occurs partially due to the influence of ϕ_q .

An increase in R_n often leads to an increase in H , E , or both. The increase in H acts to increase h , while the increase in E tends to decrease the LCL (by increasing q). Therefore, precipitation is possible in a wider range of FA conditions, as shown in Figure 2.5. Because atmospheric humidity is less sensitive to direct changes in E than to changes in entrainment [Juang *et al.*, 2007; Siqueira *et al.*, 2009; van Heerwaarden *et al.*, 2009], the increase in h dominates. Thus, an increase in R_n generally leads convection to be triggered at a greater h . If only the EF is changed, however, the LCL is more responsive than h . As a result, increasing the EF through an increase in g_{\max} (such as might occur due to changes in canopy height, leaf area index, or land use) increases the conditions under which the stationary state includes rain (Figure 2.5).

Soil moisture limit cycles with period exceeding one day occur for only a limited region of parameter space (<5% of the plane in Figure 2.5). The period here refers to the number of days between rainfall events. In these cases, the minimum time

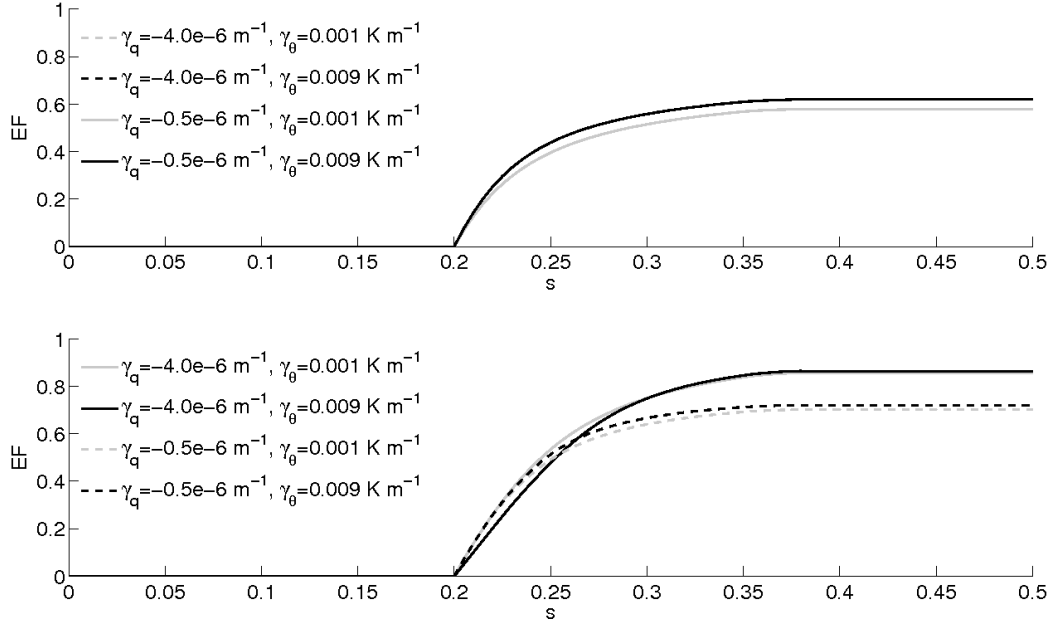


FIGURE 2.6: Daily mean evaporative fraction (EF) versus soil moisture (s) for various combinations of end-member profiles for free atmospheric temperature and humidity. In a) the dry air entrainment feedback is artificially shut off by keeping VPD equal to its early-morning value when determining surface partitioning, and in b) the dry air entrainment feedback is included. Rainfall occurrence is suppressed in both simulations.

between rain events is always greater than one day. A few days after a rainfall event, the atmospheres of these limit cycles still support a crossing of the ABL and the LCL despite the low surface heating. However, this low surface heating is not conducive to convection (i.e. the $-z/L > 5$ condition is not met). Rainfall events cannot occur until the soil becomes sufficiently dry, leading to large H and elevated h . For a given FA humidity profile, the limit cycle period increases quasi-parabolically with γ_θ , matching the rate of increase of afternoon h .

2.4 Dry air entrainment influence on surface partitioning

The dry air entrainment feedback mentioned in the introduction significantly affects the shape of the rain-no rain boundary in Figure 2.5. If it is shut off (i.e. VPD is held at its early morning value when determining surface energy partitioning), sensitivity of precipitation occurrence to atmospheric humidity increases. The “boundary line” between rainy and dry conditions becomes even steeper. Figure 2.6 illustrates why, showing the mean daily EF as a function of s for various combinations of end members for FA temperature and humidity profiles. If entrainment does not affect surface energy partitioning, the EF is far less dependent on FA humidity than on FA temperature conditions. The dry air entrainment feedback, included in the curves in Figure 2.6b, increases EF through the increase of VPD over the course of the day. Due to the direct influence of FA humidity on the amount of entrainment, the resultant EF is also more dependent on FA humidity than on FA temperature conditions. Thus, the dry air entrainment feedback makes the rain/no-rain state less dependent on the FA humidity profile by allowing surface partitioning to partially compensate for changes in this profile.

Figure 2.6 also illustrates why the stationary state is insensitive to initial soil moisture conditions only for sufficiently high s . The EF curve is steep near the wilting point. If s starts near this point, the LCL remains elevated throughout the day and rain is only possible under the most favorable conditions. As initial conditions move further away from the wilting point, the boundary line between rainy and non-rainy states moves closer to that shown in Figure 2.5. Nonetheless, soil moisture influences the possibility of rainfall only under a limited combination of FA parameters. Over only seven percent of the plane does a soil at s^* create a different rain/no-rain outcome than a soil at s_w .

2.5 Conclusions

Using a coupled surface-ABL model and a simplified parametrization for rain occurrence, we can test the relative effect of surface energy partitioning and free atmospheric parameters on the soil moisture state with some tractability. For a given set of ‘permanent’ FA parameters, the ecosystem always evolves towards either a completely dry state (desertification) or a limit cycle with daily or multi-day rainfall (wet-tropical). The transition between rainy and non-rainy states is a sharp function of FA parameters, and is more sensitive to the FA humidity profile than the FA temperature profile. The response of surface energy partitioning to dry air entrainment decreases sensitivity to the FA humidity profile. To resolve the effect of the free atmosphere on convective rainfall occurrence, it is necessary to account for both the rate of entrainment and the response of surface energy partitioning to the ABL state.

Under more realistic temporally variable FA conditions, the occurrence statistics of convective rainfall and resulting soil moisture distribution are a function of the distributions of FA temperature and humidity profiles and their associated rain/no rain state. If those distributions are concentrated near the boundary between rainfall and non-rainfall supporting conditions, small changes in the boundary line (such as can be caused by changes in land surface conditions or seasonal changes in incoming radiation) may have a large effect on the resulting potential for convective precipitation occurrence.

Spatial Patterns and Rainfall Feedbacks Determine Drought Sensitivity of Patterned Vegetation

3.1 Introduction

In many arid and semi-arid regions, vegetation patches form spatial patterns such as spots or labyrinthine stripes. Such patches have been modeled using an activator-inhibitor or Turing-type model, wherein enhanced infiltration capacity beneath vegetated sites and/or extensive lateral root networks promote patch growth at small scale, but inhibit it at larger scale because of competition for water [*HilleRisLambers et al.*, 2001; *Barbier et al.*, 2006]. The models indicate that pattern type depends on the average annual rainfall rates [*Rietkerk et al.*, 2002], and that significant hysteresis exists in these systems [*van de Koppel et al.*, 2002; *Rietkerk et al.*, 2004]. These factors have sparked significant interest in using pattern morphology as indicators of desertification, capable of identifying systems that are close to an ‘irreversible’ shift in vegetation cover towards bare soil. While the role of average annual rainfall rates on steady-state vegetation development has been studied repeatedly, two inter-related issues have not yet been fully addressed: the effect of variable rainfall

dynamics and concomitant transient behavior in biomass and vegetation morphology, and the existence of feedbacks between the land surface and rainfall in patterned vegetation systems. In this Chapter, these two issues are studied in the context of vegetation patterns occurring in southwestern Niger, where both spotted and banded patterns have been observed [*Barbier et al.*, 2006; *Valentin and d’Herbes*, 1999] and are expected to be common [*Deblauwe et al.*, 2008].

With regards to the first issue, little is known about the timescales of vegetation response to shifts in rainfall regimes such as those that might be associated with climatic variability. Over scales larger than those of the patterned vegetation distribution, several studies have found that the greening of Normalized Difference Vegetation Index (NDVI) measurements over the Sahel since the drought ending in the mid-1980’s can be partially, though not completely correlated to rainfall on timescales of less than one year [*Hermann et al.*, 2005; *Ollson et al.*, 2005]. However, few records exist of the timescales at which vegetation, and particularly patterned vegetation responds to decreases in rainfall due to drought. *Barbier et al.* [2006] noted that fully vegetated cover under both grazing and water stress changed to spotted vegetation patterns over the course of several decades. *Deblauwe et al.* [2011] also observed changes in pattern types in Sudan between remote sensing observations 20 years apart and spanning a drought. The dynamics of the change in pattern, including the fractional timespan within the 20 years over which the pattern change occurred, are not known. In the absence of additional field data, one can nevertheless explore the drought sensitivity of patterned vegetation via model runs. What is the model-predicted ‘inertia’ of the vegetation pattern? That is, how do drought timing and duration influence the size and speed of vegetation pattern response? Is it appropriate to compare steady state model results to observed patterns without taking into account the history of how those patterns evolved?

Answering such questions is further complicated by the possibility that the veg-

etation cover itself affects the amount of rainfall. Depending on atmospheric conditions, higher evapotranspiration (ET) associated with wetter soils may wet the atmosphere sufficiently to enhance rainfall (a positive feedback). Alternatively, under some conditions, increased turbulent mixing in the atmospheric boundary layer associated with higher sensible heat fluxes from dry soils may cause the initiation of convective rainfall (a negative feedback). A sensitivity analysis using global circulation models (GCM) showed that soil moisture-precipitation feedbacks are most common in areas that are neither very wet (when evapotranspiration is sufficiently high to generate rainfall independent of soil moisture), nor very dry (when the atmosphere is too dry to generate rainfall under any conditions) [*Koster et al.*, 2004]. Based on a number of GCM runs, feedbacks are therefore expected to exist in the Sahel [*Koster et al.*, 2006]. However, there is still some disagreement about the sign of these feedbacks [*Taylor and Ellis*, 2006; *van den Hurk and van Meijgaard*, 2010]. Because the strength of these feedbacks depends on the soil moisture and surface energy partitioning, changes in vegetation cover can also be associated with changes in rainfall. Vegetation can induce precipitation feedbacks by changing the surface energy balance in two main ways [e.g. *Dekker et al.*, 2010]: a) by changing the surface albedo and therefore the net radiation and b) by changing the latent and sensible heat fluxes to the atmosphere resulting from a given amount of available radiation and soil water. The feedbacks operating through each of these pathways are referred to here as the ‘radiative feedback’ and ‘evapotranspiration feedback’, respectively.

Only a handful of studies have considered vegetation patterns in the context of dynamic rainfall and these two vegetation-precipitation feedbacks. As shown in Table 3.1, most studies did not include either vegetation-precipitation feedbacks or precipitation dynamics, and no studies have included both. Table 3.1 is not meant to be an exhaustive listing of all patterned vegetation studies, but a sample of how precipitation-vegetation patterning is currently being treated.

Table 3.1: Treatment of precipitation feedbacks and dynamics in some patterned vegetation studies

Study	Precipitation Feedbacks	Precip. Dynamics
<i>HilleRisLambers et al.</i> [2001]	None	None
<i>Rietkerk et al.</i> [2002]; <i>van de Koppel et al.</i> [2002]	None	None
<i>Kefi et al.</i> [2008]; <i>Thompson et al.</i> [2008]	None	None
<i>Scheffer et al.</i> [2005]	Parameterized relationship	None
<i>Dekker et al.</i> [2007]	Evapotranspiration feedback	None
<i>Janssen et al.</i> [2008]	Monsoon strength feedback, dependent on radiative feedback	None
<i>Guttal and Jayaprakash</i> [2007]	None	Wet and dry seasons
<i>Ursino and Contarini</i> [2006]	None	Wet and dry seasons
<i>Kletter et al.</i> [2009]	None	Intermittency

Several studies have considered the role the vegetation-infiltration relationship supporting patterning plays in determining the size of the vegetation-precipitation relationship [*Scheffer et al.*, 2005; *Dekker et al.*, 2007; *Janssen et al.*, 2008]. *Dekker et al.* [2007] used a linear relationship between precipitation amount and evapotranspiration to show that local feedbacks between biomass and soil moisture may cause large-scale vegetation-precipitation feedbacks to be underestimated by as much as 35%. Since far smaller shifts in steady-state rainfall can cause changes in spatial vegetation pattern morphology [e.g. *Rietkerk et al.*, 2002; *Thompson et al.*, 2008], such a large feedback implies coupled vegetation-rainfall models are necessary before any quantitative inferences can be made purely from spatial vegetation patterns. *Janssen et al.* [2008] performed a similar study in the context of precipitation feedbacks occurring through large-scale monsoon strength variation.

Vegetation-precipitation feedbacks depend on a large number of interacting processes that create a highly non-linear relationship between the land surface and the boundary layer structure, which controls the predisposition to precipitation occurrence [*Ek and Holtslag*, 2004; *Santanello et al.*, 2007; *van Heerwaarden et al.*, 2009]. As a result, land surface-precipitation feedbacks are only possible under a limited range of free atmospheric conditions (see also Chapter 2). These conditions are limited further by the seasonal nature of the hydrologic cycle in the Sahel, which essentially terminates the feedback mechanisms at the start of the dry season. Ear-

lier estimates of the influence of precipitation feedbacks on patterned vegetation may therefore have overestimated the size of the vegetation-precipitation feedback. Consideration of the non-linearities associated with coupled land surface-atmospheric processes, as well as seasonality, is therefore a logical extension of previous studies.

In this Chapter, a one-dimensional atmospheric boundary layer (ABL) model is coupled to a patterned vegetation model to explore the sign and size of vegetation-precipitation feedbacks under temporally variable forcing parameters. The coupled model is used to address two questions: *a)* How and how fast do modeled vegetation patterns respond to changes in rainfall regime? (Q1) and *b)* How do vegetation-precipitation feedbacks, both those acting through changes in the radiative balance and those acting through changes in evapotranspiration, affect this response? (Q2). To address these questions, a stationary state for the coupled model is perturbed with changes in rainfall depth of different sizes to simulate initiation of a drought. The response of both vegetation and dynamic precipitation is then analyzed in the context of Q1 and Q2.

3.2 Methods

3.2.1 Conceptual framework

Coupling vegetation-infiltration feedbacks in patterned systems to precipitation variability is difficult due to the large differences in relevant scales between the two processes. Explicitly resolving all relevant scales is computationally infeasible. Instead, a minimalist model that captures certain processes without explicitly resolving them is proposed. As a starting point for building such a minimalist model, Figure 3.1 illustrates the temporal and spatial scales associated with the key processes that influence vegetation and rainfall fields. Overland water transport between bare soil and vegetated patches allows the increased infiltration over vegetated sites that permits patches to persist, a transport process that requires seconds to minutes. A

minimalist model of rainfall at a given site requires resolving the development of the ABL over the course of the day. The intersection of the evolving ABL with the level of free convection is a necessary, though not sufficient, condition for rainfall to occur [Findell and Eltahir, 2003]. Once initiated, clouds over an area of tens to hundreds of kilometers may develop into a mesoscale convective system. Their growth and spatial movement is determined by land surface conditions over the extent and duration of the system. Seasonal variability determined by regional climate affects the ability of the turbulent boundary layer to grow to a height promoting rainfall occurrence. In the Sahel, climate is dominated by a single monsoon season lasting roughly from April to October. This climatic variability can be included in a one-dimensional atmospheric boundary layer model by appropriately varying the forcing parameters that modulate lateral heat and moisture transport and entrainment of warm, dry air at the top of the ABL. Such parameters can be estimated from radiosonde measurements, obviating the need for detailed climatic simulations. However, these parameters are controlled by regional climate and atmospheric circulation on scales of hundreds to thousands of kilometers.

In this study, only local-scale vegetation-precipitation feedbacks are considered. The model used here cannot account for feedbacks due to changes in monsoon strength, such as those studied by *Janssen et al.* [2008]. The sensitivity of the monsoon strength to vegetation cover morphology operates over far larger spatial scales than those considered here. At the spatial scales of tens and hundreds of kilometers that are relevant to the monsoon strength, much variability in vegetation morphology is expected. Indeed, vegetation patterns are unlikely to cover the entire zone of influence (see for example, the variability in the map of predicted pattern occurrence in *Deblauwe et al.* [2008]). To account for local-scale feedbacks, a one-dimensional ABL model driven by large-scale forcing parameters determined from sounding observations is coupled to a vegetation pattern model. The vegetation pattern model of

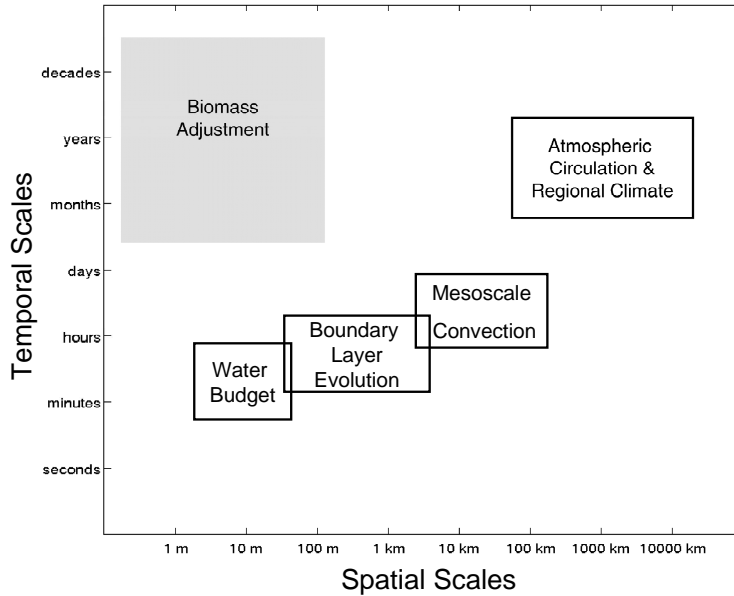


FIGURE 3.1: Spatial and temporal scales of the processes impacting vegetation patterns and rainfall occurrence. The temporal scales of biomass adjustment are unknown and are investigated. The water budget is represented by Eqs. 3.7-3.8, the boundary layer is represented by Eqs. 3.1-3.3, mesoscale convection is represented by Eq. 3.6, and biomass adjustment is dependent on Eq. 3.14. Atmospheric circulation and regional climate are represented by the parameters of Eqs. 3.1-3.2.

Kefi et al. [2008] is revised to include a radiative and an energy balance that allows prediction of the diurnal evolution of average surface sensible and latent heat fluxes, a necessary driver for the ABL and therefore the rainfall model.

3.2.2 ABL model

The surface sensible and latent heat fluxes determined by the revised vegetation pattern model are used to drive the dynamics of the atmospheric boundary layer, which is used in turn to predict rainfall occurrence. Large eddy simulation studies have shown land surface heterogeneity must be on the order of several kilometers in wavelength before the boundary layer development is affected [*Avissar and Schmidt, 1997*]. Since the heterogeneity associated with vegetation patterns occurs on scales

several orders of magnitude smaller (see Figure 3.1), it is not necessary for the boundary layer to be modeled in three dimensions. The ABL model used is equivalent to the model in Chapter 2 and is included here for completeness. A so-called slab model is used for the convective ABL, determining average values for potential temperature and specific humidity in the boundary layer and its height h throughout the day. The boundary layer is thus assumed to be sufficiently well-mixed that the temperature θ and the specific humidity q are constant. In the free atmosphere above h , both θ and q are assumed to vary linearly with height. Thus,

$$\theta(z) = \gamma_\theta z + \phi_\theta \quad (3.1)$$

$$q(z) = \gamma_q z + \phi_q \quad (3.2)$$

The two sets of slope and intercept parameters are determined by climatic conditions and are further clarified below. Warm, dry air is mixed into the boundary layer from above (through entrainment) at a rate proportional to the temperature and humidity gradients between the free atmosphere right above the boundary layer and the boundary layer itself. The bottom of the ABL is heated and moistened by surface sensible and latent heat fluxes, respectively. Figure 2.1 illustrates these assumed profiles and the fluxes driving their dynamics.

The growth of the boundary layer height h is determined by [Garratt, 1992],

$$\frac{dh}{dt} = \frac{(1 + 2A)\overline{(\theta'\omega')}_s}{\gamma_\theta h} \quad (3.3)$$

where $\overline{(\omega'\theta')}_s$ is the surface sensible heat mass flux determined as part of the surface energy balance, and A is the Tennekes parameter, defined as the ratio of the sensible heat flux at the top of the boundary layer to the surface sensible heat flux. A is assumed to be constant and is taken to equal 0.2 [Kim and Entekhabi, 1998]. As vegetation increases the latent heat flux from the surface, less energy is available for

sensible heating of the atmosphere, and the boundary layer grows more gradually. The flux of heat and humidity at the top of the growing boundary layer is proportional to the difference between the value right above the top of the ABL and that right below it (i.e. the value of the ABL itself). Conservation equations can be used to determine the dynamics of the ABL temperature and humidity,

$$h \frac{d\theta}{dt} = \overline{(\omega'\theta')_s} + (\gamma_\theta h + \phi_\theta - \theta) \frac{dh}{dt} \quad (3.4)$$

$$h \frac{dq}{dt} = \overline{(\omega'q')_s} + (\gamma_q h + \phi_q - q) \frac{dh}{dt} \quad (3.5)$$

where $\overline{(\omega'q')_s}$ is the surface latent heat mass flux. The $\overline{(\omega'q')_s}$ and $\overline{(\omega'\theta')_s}$ are related to the latent and sensible heat energy fluxes determined in Section 3.2.3 through $\overline{(\omega'q')_s} = \frac{LE}{\rho\lambda}$ and $\overline{(\omega'\theta')_s} = \frac{H}{\rho c_p}$.

Convective rainfall is only possible when the ABL height crosses the level of free convection (LFC), the height at which lifted surface parcels become buoyant. In the model, rainfall is possible only if the ABL crosses the lifting condensation level (LCL), the height at which condensation starts. To ensure parcels have sufficient buoyancy to rise the distance from the LCL to the LFC, an additional condition that $z/L \geq 5$ is imposed, where L is the Obukhov length $L = \frac{u_*^3 \theta}{\kappa_v g (\omega'\theta')_s}$ [Kader and Yaglom, 1990]. The κ_v is von Karman's constant, g is gravitational acceleration, and u_* is the friction velocity. Since no friction velocity measurements are available for patterned vegetation systems in Niger, I use half-hourly eddy-covariance observations (temporally interpolated to the model timestep) ensemble averaged over a variety of sites. The diurnal cycles of all sites are similar, providing confidence that using data from different locations is appropriate for use in this model of rainfall in the Sahel, at least in a first order estimate.

When rainfall occurs, the amount of rainfall is equal to a fraction η of the total water vapor in the atmospheric column. The height over which free atmospheric

moisture is non-zero, given by $\frac{\phi_q}{\gamma_q}$, can vary considerably depending on variations in γ_q and ϕ_q . The water column from which precipitation (R) is drawn is therefore capped at $2h$ to prevent unrealistic sensitivity to small fluctuations in the free atmospheric parameters and is given as:

$$R = \eta \int_{z=0}^{z=2h} q dz. \quad (3.6)$$

The η integrates a whole range of processes that determine rainfall efficiency, including the availability of condensation nuclei (i.e. dust and other aerosols), cloud depth, and age. The effects of these combined factors are difficult to model, and they are lumped into a single parameter here.

For simplicity, each rainstorm is assumed to be distributed over two hours. Although this is almost certainly a gross simplification of the actual rainfall description, modeling storm distribution is beyond the scope of this simple model. Nevertheless, by having rainfall occurrence and amount depend on vegetation and climatic conditions via surface and free atmospheric fluxes, respectively, the model captures the processes and timescales that determine vegetation-precipitation feedback occurrence. At night, the ABL collapses and becomes stable. It is assumed that no rainfall occurs at night, another idealization of reality.

3.2.3 *Surface cover model*

The vegetation pattern model, revised from *Kefi et al.* [2008] to include an energy balance and to account for drought-adaptation mechanisms, consists of three state variables, the biomass P , the subsurface water content W , and the surface water content O . The dynamics of surface water are modeled according to

$$\frac{\partial O}{\partial t} = R - \alpha_0 \frac{P + k_2 W_0}{P + k_2} O + D_O \nabla^2 O, \quad (3.7)$$

where O is increased by precipitation of rate R , and continually loses water to infiltration at a rate $\alpha_0 \frac{P+k_2W_0}{P+k_2}$. The α_0 is the maximum infiltration rate, k_2 is the saturation constant of infiltration, and W_0 is the relative infiltration rate over bare soil. The infiltration rate is taken proportional to the amount of surface water O . Overland flow of water is modeled as a diffusive process with diffusivity D_0 . Although this is a poor approximation of the physical processes governing surface flow, the flow is assumed sufficiently fast relative to other processes that the exact routing mechanism of water from the soil to the vegetation does not impact the total amount of infiltrated water in vegetation patches and therefore does not influence the patch growth.

The evolution of subsurface water is modeled as,

$$\frac{\partial W}{\partial t} = \alpha_0 \frac{P + k_2 W_0}{P + k_2} O - E_t - E_s - r_w W + D_W \nabla^2 W, \quad (3.8)$$

where W is gained from infiltration, but lost due to transpiration E_t , soil evaporation E_s , and deep soil drainage at a rate $0.4r_w W$. Lateral transport is once again modeled as a diffusive process, where D_W is the diffusivity of sub-surface water. Deep soil drainage is adapted from the standard practice of using $r_w W$ to represent losses due to bare-soil evaporation and deep drainage. *Dekker et al.* [2007] found about 40% of those losses could be attributed to drainage. E_t and E_s are modeled by calculating the latent heat of transpiration and soil evaporation. The Penman-Monteith equation is used in each case, but uses different descriptions of the surface conductance for transpiration and evaporation, respectively. The canonical form of the Penman-Monteith equation is,

$$LE = \frac{\Delta(R_n - G) + \frac{\rho c_p VPD}{r_a}}{\Delta + \gamma(1 + \frac{r_s}{r_a})}, \quad (3.9)$$

where R_n is the net radiation at the surface, G is the ground heat flux, ρ and c_p are the density and specific heat capacity of air, respectively, and VPD is the

vapor pressure deficit. Δ is the slope of the Clausius-Clapeyron equation relating the saturated vapor pressure of water to temperature, and γ is the psychrometric constant, $\gamma = \frac{c_p P_s}{0.622\lambda}$, where P_s is the surface pressure and λ is the latent heat of evaporation of water. The r_a is the aerodynamic resistance, while r_s is the surface resistance, the inverse of the surface conductance. When calculating the transpiration LE^T , the surface conductance is the stomatal conductance, $r_s = r_s^{Tr} = 1/g_s^{Tr}$, while $r_s = r_s^{Es} = 1/g_s^{Es}$ when using Eq. (3.9) to calculate the soil evaporation. The radiative calculations necessary for the use of Eq. (3.9) are further detailed below. Once the total latent heat is determined, it can be converted to the total height of water evaporated or transpired,

$$E_t = \frac{LE^t}{\lambda \rho_{H_2O}} \quad (3.10)$$

$$E_s = \frac{LE^s}{\lambda \rho_{H_2O}} \quad (3.11)$$

where ρ_{H_2O} is the density of water.

The stomatal conductance g_s^{Et} captures the vegetation response to water stress. It is determined by calculating the leaf conductance as a function of water stress (specifically, W and the vapor pressure deficit VPD) and upscaling it to the canopy level depending on the leaf area index. The leaf area index is calculated as $\alpha_1 P$, where α_1 is the amount of leaf area per unit biomass. The total stomatal conductance is given by,

$$g_s^{Et} = g_{max}^{Et} \frac{W}{W + k_1} (1 - m \log(VPD)) \alpha_1 P. \quad (3.12)$$

where g_{max}^{Et} is the maximum stomatal conductance per unit leaf area, k_1 is a saturation constant of water stress, m controls the rate of decrease in conductance with increased vapor pressure deficit VPD (in kPa). The saturation function $\frac{W}{W+k_1}$ is commonly used to represent patterned vegetation response to water stress [e.g. *HilleRisLambers*

et al., 2001; *van de Koppel et al.*, 2002; *Rietkerk et al.*, 2002]), while $1 - m \log(VPD)$ has been found to be an appropriate description of the rate at which stomata close when atmospheric water demand is high (to prevent excessive water loss) across many species [*Oren et al.*, 1999]. This function has also recently been shown to be consistent with stomatal optimization theories [*Katul et al.*, 2009; *de Boer et al.*, 2011]. The soil surface conductance $g_s^{E_s}$ used to estimate E_s is given by

$$g_s^{E_s} = g_{max}^{E_s} \frac{W}{W + k_1} \left(1 - \frac{P}{P + k_3}\right), \quad (3.13)$$

where $g_{max}^{E_s}$ is the maximum bare soil conductance and k_3 is the saturation constant for the evaporation reduction function due to shade from biomass.

Plant growth and movement are modeled as a balance between assimilation and respiration,

$$\frac{\partial P}{\partial t} = (g_{CO_2} c C_1 \alpha_1 P - Resp(T_{air}) P) \frac{1}{\tau(W)} + D_P \nabla^2 P \quad (3.14)$$

where g_{CO_2} is the stomatal conductance with respect to CO_2 , c is the concentration gradient of CO_2 between the atmosphere and the intercellular space of the stomata, and C_1 is a conversion factor between carbon gain and biomass growth. The $Resp(T_{air})$ is the autotrophic respiration as a function of air temperature T_{air} (in Celsius). The $\tau(W)$ accounts for drought-adaptation mechanisms within the vegetation [*Guttal and Jayaprakash*, 2007]. Lastly, D_P is the diffusivity of the biomass spread process. Although representing biomass spread as a purely diffusive process is a simplification, *Thompson et al.* [2008] showed that the energetic modes of the vegetation morphology do not change significantly if a more realistic kernel-based method is used. The properties and closure state of the leaf stomata influence both transpiration and assimilation, such that g_{CO_2} and g_{H_2O} are linearly proportional

$$g_{CO_2} = \nu \frac{Tr}{q - q^*} \quad (3.15)$$

where ν is the ratio of the stomatal conductance with respect to CO_2 to the stomatal conductance with respect to water, q is the near-surface (here, boundary layer average) specific humidity, and q^* is the specific humidity at saturation. Respiration rates depend on temperature according to

$$Resp(T_{air}) = R_{10} Q_{10}^{\frac{T_{air}-10}{10}}. \quad (3.16)$$

The near-surface air temperature varies over the course of the day. By definition, $T_{air} \approx \theta$ near the surface. The use of $\tau(W)$ prevents vegetation from dying during each dry season by accounting for seasonal reduction in metabolic activity [Guttal and Jayaprakash, 2007] given as

$$\frac{1}{\tau(W)} = \frac{1}{4} \frac{W^2 + fk_4}{W^2 + k_4} \quad (3.17)$$

, where k_4 is a saturation constant with respect to subsurface water and f is the metabolic activity in the complete absence of water. Night-time biomass growth is assumed to be negligible. To prevent excessive fluctuations, plant biomass is updated daily, at a much coarser timescale than the ABL and water balance models.

The radiation driving transpiration and evaporation is determined by performing a full energy balance at each point in space. The net radiation $R_n(t)$ is given by

$$R_n(t) = (1 - \alpha)R_s(t) + \epsilon_s(\epsilon_a\sigma T_{air}^4 - \sigma T_s^4) \quad (3.18)$$

where α is the surface albedo, $R_s(t)$ is the shortwave radiation, ϵ_s is the surface emissivity, ϵ_a is the atmospheric emissivity, σ is the Stefan-Boltzmann constant, and T_s is the surface temperature. The terms on the right-hand side of Equation (3.18) describe the net shortwave radiation, the downward longwave radiation and the upward longwave radiation, respectively. The $R_s(t)$ is calculated based on astronomical equations, which are described in the appendix. The surface albedo depends on surface vegetation cover and is lower for more vegetated soils. Bare soils in the Sahel are

taken to be lighter than their vegetated counterpart. Therefore, albedo is linearly interpolated between $\alpha = 0.25$ at $P=0$ and $\alpha = 0.15$ at $P=25 \text{ g m}^{-2}$. For clear sky conditions, ϵ_a depends on the air temperature and air humidity as described elsewhere [Brutsaert, 1975]. Surface temperature is evolved by noting that the surface sensible heat flux H depends on the gradient between surface and air temperatures

$$H = \frac{\rho c_p}{r_a} (T_{air} - T_s) \quad (3.19)$$

where ρ and c_p are the density and specific heat of air, respectively. The atmospheric resistance r_a is modeled as $r_a = \frac{\log \frac{h_{ra}}{z_o}}{K_v u_*}$, where h_{ra} is the surface layer height, and z_o is the surface roughness height. The roughness height depends on canopy height h_c , $z_o = 0.1h_c$. The canopy height is assumed to be proportional to biomass, $h_c = \frac{5}{3}P$. H is determined as the residual of the surface energy balance,

$$H = R_n - \lambda \rho E_t - \lambda \rho E_s - G \quad (3.20)$$

G is the ground heat flux, and is assumed to equal $0.15R_n$, λ is the latent heat of vaporization of water; λ and ρ are used to convert the latent heat fluxes from mass rates to energy rates. Equations 3.18, 3.19, and 3.20 form a coupled system for R_n , H , and T_s . The values for the vegetation parameters are summarized in Table 3.2.

3.2.4 Model parameterization

The coupled model is parameterized such that the final model contains a stationary state in which the biomass forms spatial patterns at a seasonal rainfall rate near 365 mm/year, or 1 mm/day on average. This is a typical rainfall rate used in patterned vegetation models [e.g. Rietkerk *et al.*, 2002]. For the vegetation component of the model, this is accomplished by altering the α_0 , $g_{max}^{E_t}$ and $g_{max}^{E_s}$ parameters within a plausible range to achieve the typical patterns reported for the Sahel. Note that α_0 and $g_{max}^{E_t}$ are species-dependent, while $g_{max}^{E_s}$ is soil-dependent. Other vegetation

Table 3.2: Parameter values used in surface cover model

	Definition	Value	Source
r_w	Drainage parameter	0.08 d ⁻¹	Adapted from <i>Dekker et al.</i> [2007]
D_W	Diffusivity of subsurface water spread	0.1 m ² d ⁻¹	<i>Rietkerk et al.</i> [2002]
E_t	Maximum stomatal conductance	0.01 m s ⁻¹	Fitted
g_{max}	Maximum stomatal conductance	0.01 m s ⁻¹	Fitted
k_1	Half-saturation of plant water uptake	3.3 mm	Fitted
m	Conductance VPD-sensitivity	0.6	<i>Oren et al.</i> [1999]
α_1	Max. infiltration rate per unit surface water	0.2 d ⁻¹	<i>Rietkerk et al.</i> [2002]
E_s	Maximum surface conductance	0.01 m s ⁻¹	Equal to g_{max}
g_{max}	Maximum surface conductance	0.01 m s ⁻¹	Fitted
α_0	Fraction of biomass contributing to LAI	0.01 g ⁻¹ m ⁻²	Fitted
k_2	Saturation parameter for infiltration	5 g m ⁻²	<i>Rietkerk et al.</i> [2002]
W_0	Infiltration scaling for bare soil infiltration	0.2	<i>Rietkerk et al.</i> [2002]
D_0	Diffusivity of surface water spread	100 m ² d ⁻¹	<i>Rietkerk et al.</i> [2002]
k_3	Half-saturation constant for soil shading	2.5 g m ⁻²	Assumed
ν	Stomatal conductance to CO ₂ /H ₂ O	0.026 mm m ⁻² mol ⁻¹	<i>Kefi et al.</i> [2008]
c	CO ₂ concentration gradient	152 ppm	<i>Kefi et al.</i> [2008]
C_1	Biomass produced per CO ₂ assimilated	0.0017 g mol ⁻¹	<i>Kefi et al.</i> [2008]
D_P	Diffusivity of biomass spread	0.01 m ² d ⁻¹	<i>Rietkerk et al.</i> [2002]
R_{10}	Base respiration per unit biomass	0.1 d ⁻¹	<i>Kefi et al.</i> [2008]
Q_{10}	Respiration temperature sensitivity	1.60	<i>Larcher</i> [2003]
f	Drought adjustment in absence of water	0.04	<i>Guttal and Jayaprakash</i> [2007]
k_4	Drought adjustment scaling parameter	10 mm	<i>Guttal and Jayaprakash</i> [2007]
ϵ_s	Surface emissivity	0.97	<i>Brutsaert</i> [2005]
h_{ra}	Surface layer height	25 m	Assumed

parameters were derived from the models of *Kefi et al.* [2008] and *Rietkerk et al.* [2002].

To realistically parameterize rainfall and represent rainfall-related feedbacks, free atmospheric parameters (i.e. the slope and intercept of the temperature and humidity profiles) are needed. Approximately 2400 daily radiosonde profiles, distributed over 20 years, were used to determine these parameters. The data used are maintained by the University of Wyoming Department of Atmospheric Sciences. The seasonal cycle of the parameters was determined by averaging over all profiles for each day of year. This seasonal cycle is repeated from year to year. The effect of interannual variability in these parameters due to climatic fluctuations is neglected here. By keeping free atmospheric parameters constant from year to year, possible vegetation-precipitation feedbacks associated with land surface-induced changes in large-scale circulation are neglected [*Charney*, 1975]. Linking this feedback mechanism to patterned vegetation requires assuming patterns of a given time are present over very large scales (see Figure 3.1). This possibility is neglected here for simplicity. Interannual variability in precipitation amounts over variability over the West African Sahel is driven largely

by variability in the intensities and frequencies of storms rather than the length of the wet season [Grist and Nicholson, 2001]. Since the length of the wet season depends largely on the seasonal evolution of free atmospheric parameters, this provides further support for using free atmospheric forcings that are repeated every year.

The radiosoundings were taken at the Niamey airport in southwestern Niger, at mid-day (12:00 local time). The boundary layer height is lower than 1500 m by this time. Thus, linear profiles for θ and q are regressed against height for $z \in [1500, 4000]$. In southwestern Niger, long-term raingauge records indicates about 95% of the rain falls between the first day of May and the first day of October [Lebel *et al.*, 1997]. The seasonal cycle of the free atmospheric parameters, shown in Figure 3.2, roughly supports this behavior. The $|\gamma_q|$ and ϕ_q are higher during the summer monsoon season, allowing the boundary-layer to cross the LCL (which is inversely related to moisture) more readily, such that precipitation occurs for a greater range of surface fluxes. Although γ_θ is also higher during the wet season than during the dry season (allowing the boundary layer to grow higher for a given amount of sensible heating), its seasonal variability is small and shows strong fluctuations during the wet season. This is consistent with the work of Chapter 2 indicating the free atmospheric moisture parameter has a greater influence on rainfall occurrence than the free atmospheric temperature profile.

Although the conditions used to model rainfall events are necessary for the triggering and persistence of storms, they are not sufficient. Condensation nuclei size, updraft velocity, and other factors may still limit the production of rainfall. These limiting factors are generally unrelated to the average ABL state and require modeling that is too detailed to be included here. Instead, each day of the year (DOY) is assigned a binary parameter $\Pi(\text{DOY})$ that combines the limiting factors above into a single value that either allows or does not allow rainfall to occur. For each day of year, $\Pi(\text{DOY})$ is determined randomly and independently. The binary distribu-

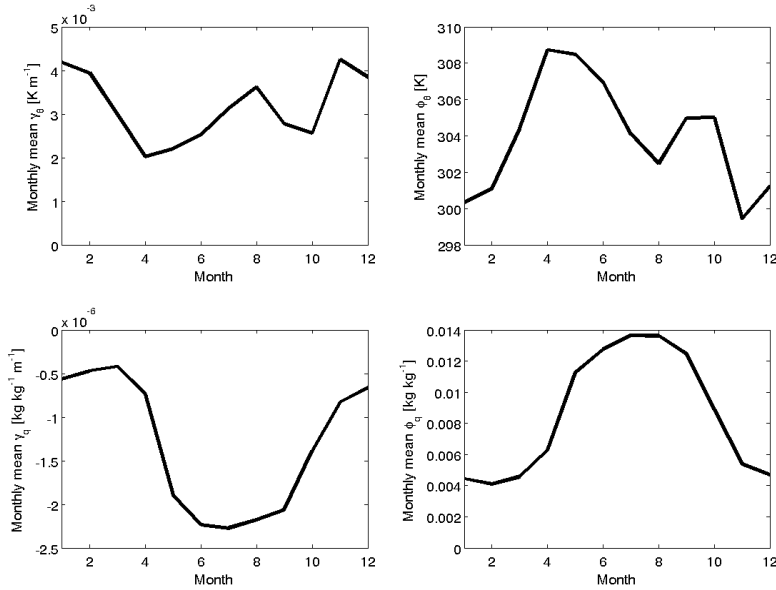


FIGURE 3.2: Seasonal cycle of the measured slope γ (left column) and intercept ϕ (right column) of the linear free atmospheric profiles for potential temperature θ (top row) and specific humidity q (bottom row) used in Eqs. 1-5 as determined from 30 years of radiosonde data collected at Niamey airport, Southwestern Niger. For comparison, late afternoon boundary layer heights are generally around 3000 m.

tion from which it is drawn is parameterized such that the total number of storms occurring each year is about 28 (depending on surface conditions), an average value appropriate for Southwestern Niger [Lebel *et al.*, 1997]. $\Pi(DOY) = 0$ during the dry season. Note that although $\Pi(DOY)$ confirms the strong seasonality of rainfall in Niger, this seasonality is also captured in the free atmospheric parameters. That is, during the dry season, the free atmospheric parameters are such that rainfall is rarely possible under any land surface conditions.

Although the conditions used to model rainfall events are necessary for the triggering and persistence of storms, they are not sufficient. Condensation nuclei size, updraft velocity, and other factors may still limit the production of rainfall. These limiting factors are generally unrelated to the average ABL state and require modeling (and a concomitant set of parameters) that is too detailed to be included here.

Instead, each day of the year (DOY) is assigned a binary parameter $\Pi(\text{DOY})$ that combines the limiting factors above into a single value that either allows or does not allow rainfall to occur. For each day of year, $\Pi(\text{DOY})$ is determined randomly and independently. The binary distribution from which it is drawn is parameterized such that the total number of storms occurring each year is about 28 (depending on surface conditions), an average value appropriate for Southwestern Niger [Lebel *et al.*, 1997]. Moreover, $\Pi(\text{DOY}) = 0$ during the dry season. Note that although $\Pi(\text{DOY})$ confirms the strong seasonality of rainfall in Niger, this seasonality is also captured in the free atmospheric parameters. That is, during the dry season, the free atmospheric parameters are such that rainfall is rarely possible under any land surface conditions.

Given $\Pi(\text{DOY})$, η_{steady} is chosen in equation 3.6 such that the rainfall intensity of the stationary state is 365 mm/year (see also Section 3.2.5 for additional justification for varying η), resulting in $\eta_{\text{steady}} = 0.33$. The steady-state annual rainfall value here is lower than the average 520 mm/year measured at the Niamey Airport in Niger from where the free atmospheric forcing parameters are derived. This discrepancy can be attributed to the high spatial variability of rainfall in Southwestern Niger. The free atmospheric parameters most likely represent a much larger spatial scale than rainfall and are still appropriate to use.

3.2.5 Analysis

3.2.6 Experimental Design

When precipitation is a system variable rather than an externally imposed forcing parameter, systematically controlling the effects of changes in rainfall amount (i.e. drought) is difficult. In the 1-D ABL model above, two factors could be varied to influence the total amount of rainfall: the free atmospheric forcings that determine when and under what conditions rainfall occurs (Eqs. 1-5), and the precipitation

efficiency η (Eq. 3.6). The free atmospheric conditions can be altered to model possible changes in large-scale atmospheric circulation that affect rainfall amounts, but doing so would require computationally intensive sampling of the full range of realistic change scenarios for not only each of the four individual parameters, but also their covariances. In contrast, modifying η (in isolation) immediately suggest how total rainfall is likely to change. Because of this tractability, η is used as a control variable throughout. In Section 3.3.1, η is scaled by different amounts to represent droughts of different sizes according to $\eta = \eta_{sc}(\eta_{steady})$. For example, when $\eta_{sc} = 0.85$, this is interpreted as a drought with an anomaly size of approximately 15% of the rainfall associated with η_{steady} , which is about 55 mm/year. Note that due to the presence of vegetation-precipitation feedbacks, this may not be the annual rainfall at any time during the drought. However, η_{sc} provides a framework for defining different drought conditions *a priori*.

As noted earlier, the vegetation state influences the development of the ABL and the resulting precipitation through two main pathways: modification of the amount of latent heating (ET feedback) and modification of the available radiative energy through the vegetation’s influence on albedo (radiative feedback). These two pathways are illustrated by the top and bottom lines of Figure 3.3. The contributions of the two mechanisms to the total feedback effect are investigated in Section 3.3.2. To determine the effects of the feedbacks, each pathway is artificially removed (in separate simulations) from the coupled system. This removal is achieved by replacing P in the above formulations with an effective vegetation cover that does not evolve in time. To allow for convenient interpretation of the sign of the feedbacks, this effective cover is designed to have a biomass less than is common even in the peak of the dry season. Its mean biomass is $\approx 3.8 \text{ g m}^{-2}$. The effective vegetation cover is used only in determining the atmospheric boundary layer development and the possibility of rainfall. As in the fully coupled model, infiltration depends on the

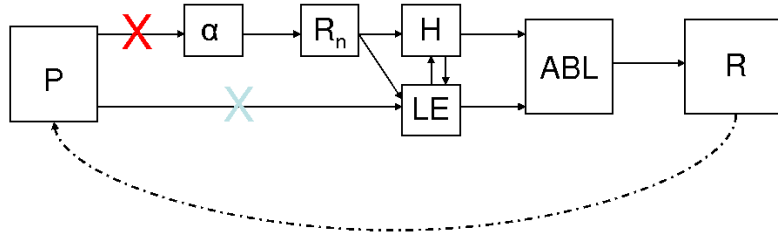


FIGURE 3.3: Key pathways of model influence of vegetation biomass on rainfall. Biomass influences albedo, which influences the surface energy R_n available for latent and sensible heating. In the ‘no radiative feedback’ simulations of Section 3.3.2, this influence is artificially removed (red cross). Biomass also has a direct influence on the total surface latent heat flux (Eqs 3.12,3.13). In the ‘no ET feedback’ simulations of Section 3.3.2, this influence is artificially removed (blue cross). The dashed line indicates rainfall also influences biomass.

dynamic vegetation. Vegetation growth depends on the values of the boundary layer VPD and T determined by the fully coupled model. Removing feedbacks solely in the determination of rainfall ensures consistency and simplifies the comparison of the full and partial vegetation-precipitation feedback cases. In the rest of this Chapter, the effective vegetation cover is referred to as the vegetation mask.

In a ‘no radiative feedback’ run, dynamic vegetation influences the energy partitioning of the ABL used to determine rainfall, but the shortwave upward radiation and the total available energy are specified according to the ‘effective’ vegetation cover mask. In ‘no ET feedback’ runs, dynamic vegetation influences the total available energy, but the partitioning of that energy into latent and sensible heating is not influenced by the evolution of vegetation, and is instead fixed according to the effective vegetation mask. Section 3.3.2 applies each of the feedback specifications to the different drought scenarios studied in Section 3.3.1 and discusses the effect of each feedback type on the total rainfall and on the resulting vegetation cover for different values of η_{sc} . The relative sizes of the ET feedback and the radiative feedback

are also discussed.

For each of the simulations in Section 3.3, the system is initiated with the same end-of-year land surface conditions for the stationary state of the case η_{steady} , representing the ‘long-term average’ rainfall. The η is then scaled by a factor η_{sc} for the entire duration of the 10-year long simulation, representing a 10-year drought. For simplicity, interannual variability is ignored throughout, except where it is generated by land surface-precipitation feedbacks.

3.2.7 Analysis Metrics

To address Q1, it is necessary to track measures of spatial vegetation pattern morphology in time. There is no unique ‘measure’ that captures all aspects of pattern morphology. Instead, all vegetation morphology patterns are characterized by two scalar measures: a) the mean biomass and b) the spatial Shannon entropy, representing the pattern type. The Shannon entropy does not depend on the absolute values of biomass, and can therefore be used as an informative scalar measure even when no absolute biomass values are known, such as when data are obtained from remotely-sensed images. The two scalar pattern measures used are entirely independent.

The Shannon entropy of a string or field represents the total information content and can be defined as

$$I_u = - \sum_{i=0}^n p_i(x) \log(p_i(x)) \quad (3.21)$$

where n is the number of bins and $p_i(x)$ is the probability that x (here biomass) belongs to bin i . As the system becomes more uniform (and $p_i(x)$ tends to a single value equal to $1/n$), the maximum weight $\log(p)$ decreases, and the measure goes to zero. To facilitate interpretation, the measure is normalized by I_u for a uniform

distribution,

$$I = \frac{\sum_{i=0}^n p_i(x) \log(p_i(x))}{-\log(n)}, \quad (3.22)$$

I now varies between 0 and 1. The normalization also reduces the dependence on the discretization of binning used in the numerical estimation of I . Again, I does not directly depend on the spatial distribution of patterns (that is, two pixels of a given biomass level interspersed with a bare pixel have the same entropy as a cluster of two pixels next to a bare patch.) Nevertheless, the measure can distinguish between different pattern types because different types have different surface area-to-volume ratios. Because biomass is generally reduced at the edges of a patch, the resulting values of $p_i(x)$ differ. This is illustrated in parts a through d of Figure 3.4, which shows the different entropies associated with the canonical pattern types, spots, labyrinthine bands, and gaps. Each of the pattern types is simulated using the model in *Rietkerk et al.* [2002]. Although spots and gaps are to some degree ‘inverse’ patterns, their associated entropy is still sufficiently different to be distinguishable. In the case of gaps, the most spatially extensive cover type (i.e. the connected areas of vegetation) still shows some variations in exact biomass level. In the case of spots, the most spatially extensive cover type consists of bare soil with biomass that is essentially zero. The only fluctuations consist of small model imperfections that are too small, relative to the total range of biomass, to affect the information content. As a result, the spatially extensive vegetation in the case of a gapped pattern contributes more to I than the spatially extensive bare soil in the case of spots, and I is distinguishably higher in the case of a gapped pattern than in the case of a spotted pattern. In part f, the observed patterned vegetation in Niger is depicted. It has a $I=0.82$, comparable to a labyrinth pattern.

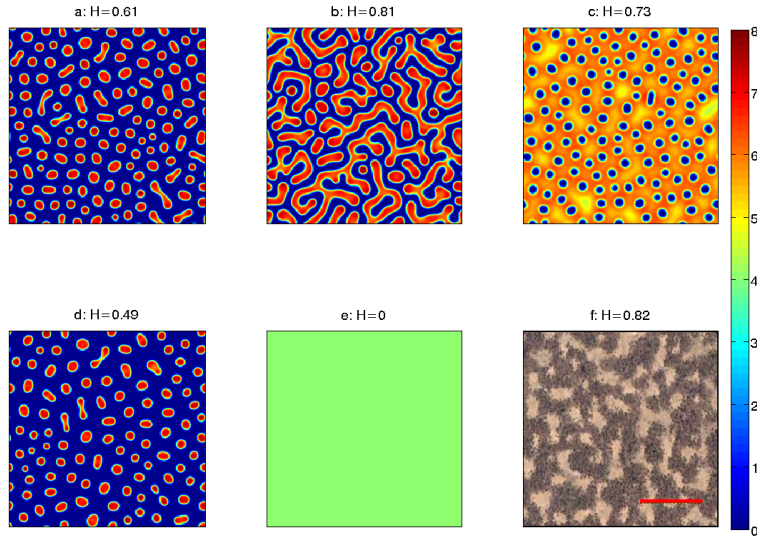


FIGURE 3.4: Shannon entropy calculated from biomass images for a) spotted vegetation patterns, b) labyrinthine vegetation patterns, c) gapped vegetation patterns, d) spotted vegetation patterns, at a lower rainfall rate than those in a, e) a uniform field and f) an image of vegetation patterns in Southwestern Niger. Each of the maps in a-d represent canonical pattern types and are simulated using the model of *Rietkerk et al.* [2002] with a 200x200 m grid using rainfall rates R of a) $R=0.75 \text{ mm day}^{-1}$, b) $R=1.00 \text{ mm day}^{-1}$, c) $R=1.25 \text{ mm day}^{-1}$, and d) 0.65 mm day^{-1} . The image in f represents vegetation patterns in Southwestern Niger, at $12^{\circ}19'54.91 \text{ N}$, $3^{\circ}10'41.76 \text{ E}$. Image taken from Google Earth, copyright 2011 Digital Globe. The red scaling line represents 100 m.

3.3 Results

3.3.1 Q1: How and how fast do modeled vegetation patterns respond to changes in rainfall regime?

The vegetation changes from a labyrinthine to a spotted pattern as the coupled system responds to drought for the case of $\eta_{sc} = 0.85$ (Fig. 3.5). During the transition, bands of vegetation become thinner until they break, leaving individual clusters of vegetation that will eventually make up the spotted pattern. The remaining bands, as well as leftover spots, die out slowly over time.

The timeseries of biomass entropy, mean (spatial) biomass, and annual rainfall

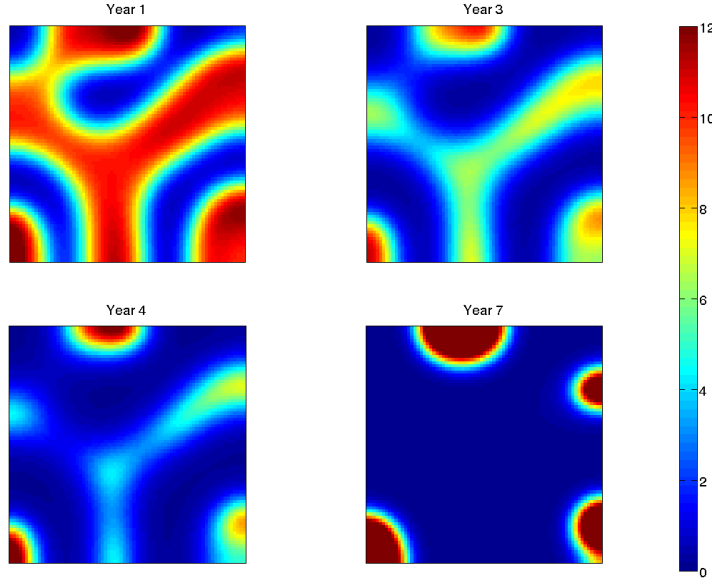


FIGURE 3.5: Biomass [g m^{-2}] spatial patterns over a grid of 75×75 m for different years after the initiation of a drought with $\eta_{sc} = 0.85$. The system evolved from a labyrinthine pattern in year 1 to a spotted pattern in year 7 through the thinning and breaking apart of bands. Remaining vegetation spots then increase in size.

amount and events for droughts of different sizes are shown in Figure 3.6. Although the rainfall decreases in all cases, biomass slightly increases when $\eta_{sc} = 0.95$; this is further discussed in Section 3.3.2. The timescale of vegetation adjustment to changes in rainfall depends on the size of the drought. While vegetation amount and spatial pattern adapt to the small reduction in rainfall resulting from $\eta_{sc} = 0.95$ (about 55 mm yr^{-1}) on timescales less than 1 year, it takes about 4 years for the vegetation to die out completely when $\eta_{sc} = 0.8$.

When $\eta_{sc} = 0.85$, both the patterns and the mean biomass require more than 10 years to equilibrate to a new steady vegetation pattern. For the first six years of the drought, vegetation biomass steadily decreases, and the vegetation cover becomes more sparse and patterns less pronounced (as reflected in the decrease in entropy). At the same time, rainfall decreases and the coupled system displays behavior that is qualitatively similar to that of the $\eta_{sc} = 0.80$ case. After the seventh year of the

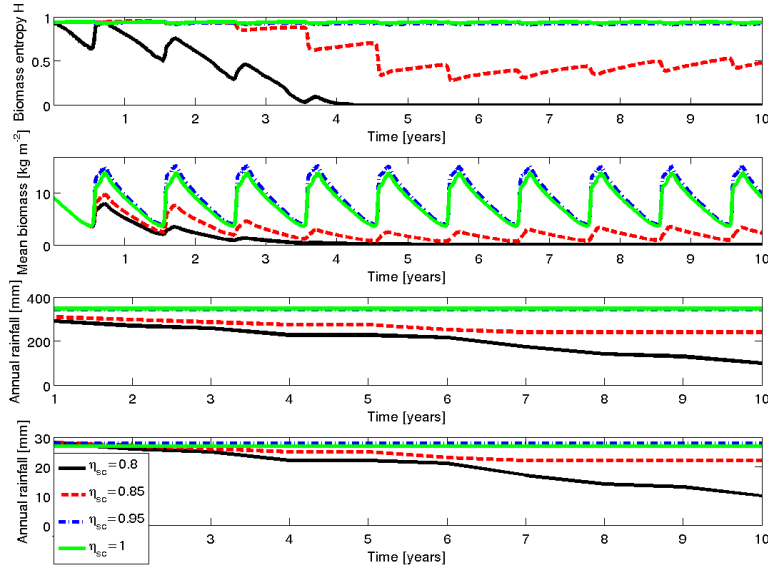


FIGURE 3.6: Evolution of the fully coupled system during drought for different reduced values of η_0 , taken to be indicative of droughts of different magnitudes. top) biomass entropy H , middle) mean biomass [g m^{-2}], and bottom) annual rainfall [mm]. For each scenario $\eta = \eta_{sc}\eta_{steady}$. All scenarios start at the same steady state with $\eta_{sc} = 1$.

drought, rainfall stops decreasing. Although the precipitation driving the vegetation dynamics is now stationary, the vegetation pattern continues to evolve for several more seasons. Moreover, the dynamics actually reverse - that is, after year 7, mean biomass and entropy both *increase* rather than continuing to decrease. This occurs due to spatial redistribution of vegetation within a cluster, changing the amount of supported biomass over time. In this case, mean wet season biomass continues to change by more than 5% for the first 8 years of drought, while mean wet season entropy continues to change by more than 5% for the first 10 years of drought.

3.3.2 Q2: How do the two types of vegetation-precipitation feedbacks affect the response?

The change of mean annual rainfall over the duration of each of the droughts indicates vegetation-precipitation feedbacks can significantly impact rainfall. For the

$\eta_{sc} = 0.80$ case shown in Figure 3.6, the rainfall in the fourth year after the initiation of the drought is 63 mm/year lower than during the first year of the drought, even though free atmospheric forcing parameters are identical in both years. This change is attributed to a decrease in the number of rainfall events occurring from 28 storms in year 1 to 22 storms in year 4, as in part d of Figure 3.6. Land surface conditions change the anomaly size of the precipitation from 17% of its long-term average value in year 1 to 35% of the long-term average in year 4. Note that the feedback represented by this simulation includes both the direct effects of changes in vegetation cover and transpiration on precipitation and the effect of changes in soil moisture and ET on precipitation. The influence of the latter can be noted from the fact that rainfall for the $\eta_{sc} = 0.80$ case continues to decrease significantly after biomass has died out. This is due to a few days with atmospheric conditions such that rainfall occurrence is very sensitive to exact soil moisture values. Due to the fluctuations of the free atmospheric parameters used here, these events happen to occur relatively early in the season. Given the dry and highly seasonal precipitation regime of Southwestern Niger, the presence or absence of individual rainfall events can significantly effect further land surface and precipitation evolution.

When $\eta_{sc} = 0.95$, one would expect that a decrease in rainfall reduces biomass. However, biomass is actually increased relative to the steady-state ($\eta_{sc} = 1$) case. Although rainfall decreases in the $\eta_{sc} = 0.95$ case, the difference in rainfall between the $\eta_{sc} = 1$ and $\eta_{sc} = 0.95$ cases is comparatively much smaller than the 5% decrease in η would suggest. The reduction in average rainfall per storm due to the decrease in the precipitation efficiency η is mitigated by the fact that a negative vegetation-precipitation feedback actually increases the number of storms in the $\eta_{sc} = 0.95$ case. This storm occurs more than halfway through the season, causing it to have a larger effect on the biomass than the reduction in precipitation due to the reduction in η during other storms, and causing the overall mean biomass to be higher for

$\eta_{sc} = 0.95$ than for $\eta_{sc} = 1.00$. However, the overall sign of the feedback indicates that in Southwestern Niger, climate is such that the potential vegetation-precipitation feedbacks are positive more often than they are negative. This can be seen by the fact that annual rainfall decreases as vegetation decreases over the course of each of the droughts. Note that the increase in biomass when $\eta_{sc} = 0.95$ is not necessarily predictive of likely (or probable) observations. It serves merely to illustrate how exact feedback dynamics as determined by the evolution of atmospheric conditions may cause counter-intuitive changes in vegetation pattern morphology to occur.

The seasonally-averaged sign of the precipitation feedback can be ‘tested’ for all values of η by explicitly removing feedbacks using the method described in Section 3.2.5 and Figure 3.3. Figure 3.7 summarizes the effects of the vegetation-precipitation feedback on mean annual rainfall, number of storms per year, and average storm depth as a function of η_{sc} . Although these values change over the course of a given drought (as seen in part c of Figure 3.6), only the average values for the first year of the drought are shown for the sake of tractability. During later years, as vegetation adapts to the new conditions, the size of the ET feedback changes in the ‘no radiative feedback’ case and vice versa. This complicates the interpretation significantly. The mean annual rainfall figure summarizes the average sign of each of the two feedback types (Figure 3.7a). The decrease in rainfall in the ‘no radiative feedback case’ relative to the ‘all feedbacks case’ implies the radiative feedback promotes rainfall for higher values of biomass, indicating a positive feedback between biomass and precipitation. The radiative feedback is consistently positive - since the state of the biomass during the wet season in the all-feedback case is higher than the constant biomass mask value used in the no-feedback case (by design), the surface albedo is lower in the all-feedback case, net radiation is higher, and surface fluxes are larger. The increased sensible heat flux causes the boundary layer to grow higher and faster, while the increased latent heat flux increases the specific humidity of the boundary

layer, decreasing the lifting condensation level. This decrease in the LCL makes the initiation of a convective event more likely. The average depth per storm is essentially unaffected by the feedback presence, as shown by the ‘no radiative feedback’ line in Figure 3.7c. Note that based on the mean biomass results of Figure 3.6, wet season biomass during the third year of drought is actually lower than the biomass mask used when $\eta_{sc} = 0.85$, and more rainfall is expected in the ‘no radiative feedback’ case than in the ‘all feedbacks’ case. This is not observed in Figure 3.6 because biomass actually increases significantly between the ‘all feedbacks’ and ‘no radiative feedback’ cases (further discussed below.)

On a seasonal scale, rainfall is also higher in the ‘all feedbacks case’ than in the ‘no ET feedback case’ with an artificially low constant biomass mask. Therefore, the evapotranspiration feedback is positive for all values of η . Because the effective biomass is higher in the presence of the evapotranspiration feedback, evapotranspiration is higher and the resulting atmospheric humidity and LCL height are lower, making the initiation of a convective rainfall event more likely.

The size of the ET feedback is smaller than the size of the radiative feedback given the compensatory effects of increased evaporation and reduced transpiration (and biomass). Transpiration increases with biomass. However, the subsequent reduction in available soil moisture and the increase in shading cause bare soil evaporation to decrease, buffering the effect of a change in biomass on total evapotranspiration. Further compensation occurs between vegetated and bare areas through the redistribution of water. Due to the lateral re-distribution of water both above and below the surface, less water is available for bare soil evaporation from bare patches when transpiration from a vegetated cluster is increased. On average, rainfall amounts differ by more than 20% between the ‘all feedback’ and ‘no feedbacks’ cases, indicating vegetation-precipitation feedbacks are a key source of rainfall even in marginal drylands with low biomass amounts of patterned vegetation.

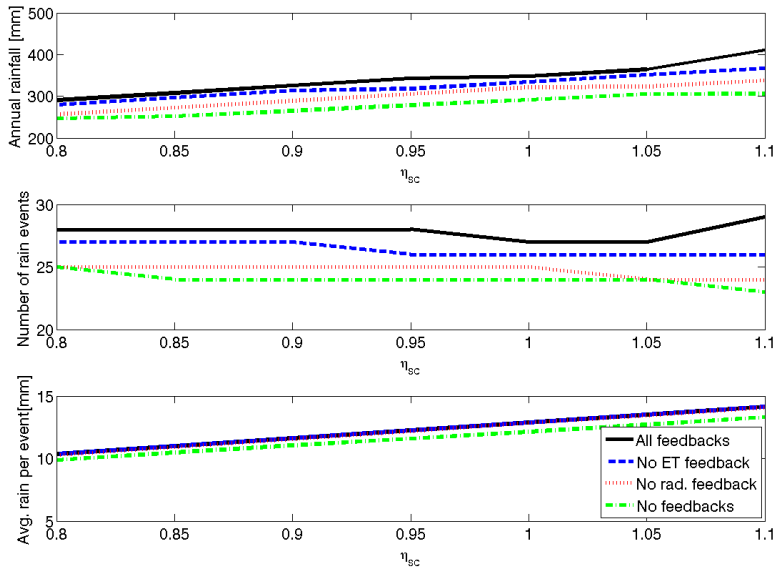


FIGURE 3.7: Rainfall statistics for the first year after the start of the drought simulation under different feedback scenarios. top) annual rainfall [mm], b) number of individual storms, c) average rainfall depth per event [mm]. The lines for the average rainfall depth per event of the ‘all feedbacks’, ‘no ET feedback’, and ‘no radiative feedback’ cases are close to overlapping. The ‘all feedbacks’ case consists of the fully coupled model as described in Section 3.2. In the ‘no ET feedback case’ and ‘no radiative feedback’ case, the biomass influence on evapotranspiration and albedo, respectively, is removed when calculating fluxes to the atmosphere, but not in calculating fluxes leaving the surface (that is, the fluxes are not physically consistent). In the ‘no feedbacks’ case, the biomass influence on both evapotranspiration and albedo is removed.

Figure 3.8 illustrates the effect of feedbacks on the response of vegetation patterns to drought. For simplicity, only a single value of η_{sc} is shown, $\eta_{sc} = 0.80$. In this case, the effect of the feedbacks actually changes after some time, though its overall effect is to speed up desertification. Only when all feedbacks are present is the biomass completely removed after five years, indicating the strong effect of the positive feedbacks. For example, in the ‘no ET feedback case’, the feedback absence is mediated by the initial increase in biomass. Even when biomass does not enhance transpiration (due to the absence of a feedback), the radiative feedback

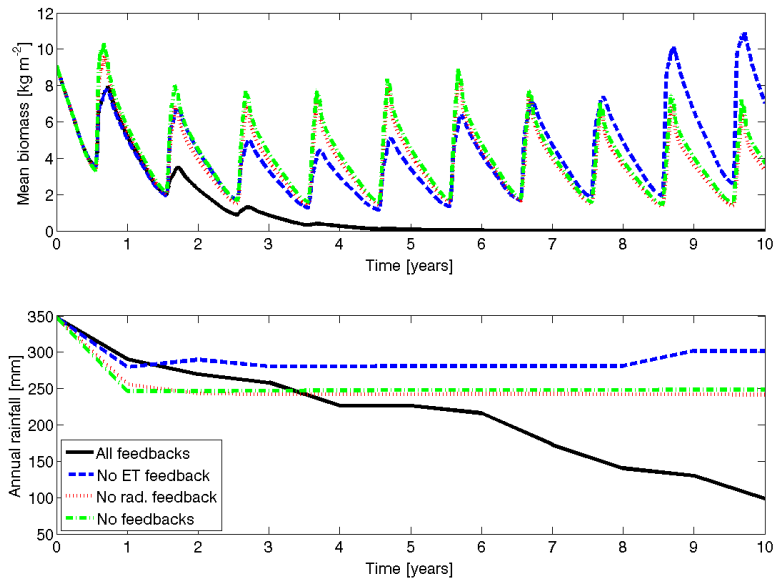


FIGURE 3.8: Evolution of coupled system after the initiation of drought at time 0 under different feedback scenarios for $\eta_{sc} = 0.80$. top) mean biomass bottom) annual rainfall. Different feedback scenarios are simulated as in Figure 3.7.

increases in size because the higher biomass levels have a greater effect on albedo. As a result, rainfall decreases when the evapotranspiration feedback is included, even though an increase in rainfall might have been expected from the positive sign of the feedback. The interaction of the different feedback processes, and their sensitivity to land surface state and history (in this case, biomass initially increases because of a few dominant negative feedback events that are affected only during the second year of drought) illustrates the difficulty of predicting their effects given a snapshot of the spatial patterns. It suggests that, to understand land surface dynamics over relatively short timescales, the effect of feedback cannot be parameterized and must be studied in reference to specific atmospheric conditions and biomass history.

3.4 Discussion and Conclusions

Field observation of the timescales of vegetation pattern response to changes in rainfall are as of yet sparse and would require at least several decades of observation. Furthermore, observations may be difficult to interpret due to variability in rainfall. In the meantime, model results may provide estimates of the inertia of vegetation pattern morphology. In this Chapter, I have shown land-atmosphere feedbacks significantly affect this inertia. The feedbacks operate primarily through changing the radiative balance of the surface and therefore the heating of the boundary layer, but to a lesser extent also through changes in evapotranspiration. Therefore, models of vegetation patterns that include vegetation-precipitation feedbacks are necessary before any quantitative inference on desertification tipping points can be made purely from spatial vegetation patterns and mean annual rainfall.

This study addresses two specific questions: Q1: How and how fast do modeled vegetation patterns respond to changes in rainfall regime?, and Q2: How do vegetation-precipitation feedbacks, both those acting through changes in the radiative balance and those acting through changes in evapotranspiration, affect this response? To answer Q1, the timescale of vegetation response to shifts in rainfall regime depends on the size of the change in rainfall. This timescale, representing the memory of the vegetation, is generally on the order of four to five years for relatively large shifts in rainfall. This is likely to be less than the duration of a drought. In West Africa, for example, a 20-yr wet period was followed by a 20-yr dry period in the second half of the 20th century [*Barbe et al.*, 2002]. The adaptation timescale of four to five years can also be interpreted as the minimum length needed for field measurements that might study pattern adaptation to drought. In certain cases (in this study, in the $\eta_{sc} = 0.85$ case), vegetation adaptations to drought are not monotonic. That is, both mean biomass and pattern entropy change from decreasing to

increasing at a certain point in the drought. This ‘overshooting’ effect implies that there is a limit to the degree of specificity with which individual images of pattern morphology can be interpreted as indicators of desertification. An increase in pattern entropy and biomass is not necessarily indicative of an increase in the available water resources. Without site-specific parameters or knowledge of site-specific rainfall history, it is impossible to know how the system will respond to different future rainfall scenarios. Put differently, the system exhibits hysteresis not only at the desertification threshold (i.e. zero biomass), but also when patterned vegetation is present due to transient effects.

To answer Q2 about the effect of vegetation-precipitation feedbacks, on a seasonally-averaged level, both the radiative and the evapotranspiration feedback pathways are positive and cause a significant fraction of seasonal rainfall. That is, a decrease in vegetation cover is exacerbated by a decrease in rainfall that causes further reductions in vegetation cover. This feedback not only increases the system sensitivity to interannual rainfall variability, but also speeds up the changes in pattern morphology associated with droughts. Note that the model used here is arguably more ‘coupled’ than reality due to the assumption of a constant value of η for each scenario. In reality, stochastic elements cause fluctuations in η that might act to counter some of the initial dry/low vegetation perturbations that are propagated by the precipitation feedbacks. Hence, the timescale of four to five years estimated in this study must be viewed as a lower bound of the adaptation timescale. This may explain why the change timescale modeled here is faster than the timescale of the field study by *Barbier et al.* [2006], in which vegetation morphology evolved from homogenous cover to a spotted pattern over the course of forty years (note also that the magnitude of drought in that study was lower than the ones modeled here).

The evapotranspiration feedback has a smaller effect on the total rainfall than the radiative feedback, as compensation processes occur in space (between evapo-

ration from bare soil patches and transpiration from vegetated patches) and time (between different days of the wet season) to limit the potential range of the total evapotranspiration contributing to rainfall. The bucket model used here to represent soil moisture may not capture all the water-based compensation effects. Transpiration is likely to access soil moisture from deeper layers than bare soil evaporation, decreasing the size of local-scale compensation. The root zone of vegetated areas are likely to extend beyond the areas with above-ground coverage [*Dunkerley, 2000; Gilad et al., 2007; Barbier et al., 2008*], amplifying the effect of compensation due to lateral re-distribution. The fact that vegetation influences rainfall primarily through influencing albedo is largely consistent with the conceptual model results of *Brovkin et al. [1998]*. This difference is particularly strong in cases with marginal biomass. In these cases, biomass has a large effect on albedo due to the cover change, but only a small effect on evapotranspiration because transpiration fluxes are small in comparison to soil evaporation fluxes.

As indicated by the seasonally-averaged sign, the sign of the vegetation cover-precipitation feedback is most often positive. However, depending on free atmospheric conditions, individual storms may be associated with a negative vegetation-precipitation feedback (i.e. rainfall only occurs when vegetation cover is low) [*Findell and Eltahir, 2003*]. *van Heerwaarden et al. [2010]* also found a negative feedback between evapotranspiration and the atmospheric system in a case study of a single wet season day in Niamey, Niger. The variability in feedback sign can have a significant influence on the system response to drought if those individual events with a negative feedback causes large storms and subsequent increases in vegetation, as occurred when biomass increased under the reduction of rainfall in case $\eta_{sc} = 0.85$, and as occurred in the scenario depicted in Figure 3.8. This possibility suggests that the system can be very sensitive to the detailed conditions of individual storms, which might affect system evolution over several years. To be able to account for

such strong sensitivity, stochastic models should be used to inform management decisions of patterned vegetation systems and to study the use of pattern morphology as indicators of ecosystem closeness to desertification.

Feedbacks have a bigger effect on rainfall and cause a larger increase in the supported biomass when η , and average biomass, is relatively high. To preserve ecosystems close to desertification, irrigation measures may therefore be more useful for gapped systems or at the beginning of a drought than for spotted systems. Making such management decisions requires some expectation of how the drought evolves. Because the system may be sensitive to the exact land surface conditions under certain atmospheric conditions, small fluctuations in η driven by essentially stochastic factors (such as the availability of aerosols) and interannual variability in atmospheric forcings can cause large changes in expected system evolution, and differing implications for ecosystem management.

Conclusions

4.1 Summary of Results

In Chapter 2, the coupled soil moisture-rainfall model was applied to a wide variety of free atmospheric parameter combinations. For each parameter combination, free atmospheric conditions were assumed to be constant in time, taking advantage of the expected auto-correlation of free atmospheric conditions from day to day. Three canonical regimes emerged: free atmospheric parameters for which rainfall never occurred (i.e. a desert-like regime), free atmospheric parameters for which rainfall occurred every day (i.e. a tropical regime), and free atmospheric conditions for which a continuously repeating pattern developed in which rainfall occurred every few days. In this last case, a negative soil moisture-precipitation feedback occurs - soil moisture is increased after rainfall, and no precipitation is possible until evapotranspiration and drainage effects have decreased soil moisture below some threshold level. The exact boundary line between the different scenarios varies depending on land surface and initial soil moisture conditions. Free atmospheric parameters that allow rainfall only for very high initial soil moisture conditions correspond to conditions under

which positive feedbacks are possible.

The distribution of the different cases suggest that the possibility of feedback occurrence is more sensitive to free atmospheric humidity conditions than it is to free atmospheric temperature conditions. This sensitivity is partially counteracted by the effect of dry air entrainment, which influences the diurnal evolution of boundary layer humidity, on surface energy partitioning. The sensitivity of the surface energy partitioning to humidity may well vary with land cover (particularly, the presence or absence of vegetation), implying that not only the occurrence of feedbacks, but also the interannual variability of this occurrence, may change with land cover in certain regions.

This rainfall framework was also coupled to a vegetation spatial pattern model in Chapter 3, to investigate how feedbacks mediate the vegetation spatial pattern response to drought. This is arguably the opposite of what is commonly done - rather than seeking to understand how precipitation feedbacks may influence the effect of a change in land cover on precipitation [e.g. *Brunsell, 2006; Juang et al., 2007*], we seek to understand how precipitation feedbacks may influence the effect of a change in precipitation on land cover. Vegetation-precipitation feedbacks amplify the response of spatial vegetation patterns to drought resulting in a vegetation morphology that changes more quickly, and responds to relatively smaller changes in rainfall regime. The results of Chapter 3 also indicated that in the Sahel, changes in the surface energy balance due to changes in albedo contribute more to rainfall than changes in evapotranspiration.

As Chapter 2 suggested, the overall sign and strength of the vegetation-precipitation feedback depends on free atmospheric conditions and their variability. In the Sahel, the overall sign of the feedback is positive, but individual rainfall events may be associated with a negative feedback. Because of the relatively small annual number of rainfall events, and because of the strong system sensitivity to water availabil-

ity, such isolated negative-feedback events can significantly influence the vegetation pattern evolution. The occurrence frequency of these negative feedback events depends on the exact day-to-day variability of free atmospheric conditions. Depending on interannual variability of these free atmospheric conditions, the overall feedback may even be hypothesized to be negative in isolated years. To capture the seasonal cycle of precipitation in the Sahel, Chapter 3 used thirty years of radiosonde observations. However, the source data was not of sufficient quality to inspect interannual variability. The application in Chapter 3 therefore illustrates how the availability of accurate forcing data can limit the applicability of the intermediate-level model built in this thesis.

4.2 Future Work

4.2.1 *Rainfall Model*

The rainfall model simulates a one-dimensional convective boundary layer. As such, it ignores the effect advection may have on boundary layer development. In some cases, deeper boundary layers may advect over more shallow, locally developing boundary layers. In such cases, the effect of advection on potential rainfall occurrence is sufficiently dramatic that local surface conditions can no longer be said to have caused rainfall.

In some cases, moisture may be advected over the course of the day that contributes above and beyond surface-derived moisture, but does not overwhelm it. Such lateral transport of moisture cannot be accounted for in the current model. Because the evolution of the boundary layer height is coupled only to the atmospheric temperature profile, and not to the humidity profile, it is possible to account for advection of moisture into the well-mixed boundary layer by simply adding another term to the budget equation for the average humidity q . Such a term adds a degree of freedom to the model, but as such it complicates interpretation and increases data

requirements. Much like a simple relationship was found between early-morning humidity and the surface intercept of the free atmospheric humidity profile, it may be possible to form a simple relationship between the amount of moisture advected and the free atmospheric humidity profile (at least for a specific region). Results from mesoscale or regional climate models may be used to inform such a relationship. Alternatively, global re-analysis datasets have the advantage of containing previously compiled records covering a long timespan. However, they are unlikely to have sufficiently high spatial resolution (on the order of hundreds of kilometers) for many applications.

Another drawback of the current feedback model is its inability to determine whether rainfall actually occurs, given that the boundary layer has passed the level of free convection. This depends on the detailed cloud dynamics of the storm and cannot be captured in a model without any cloud dynamics. Indeed, even the most sophisticated atmospheric models often rely on empirical adjustment factors to theoretical model predictions to ensure realistic precipitation behavior. In the context of the intermediate-level model of this thesis, stochastic simulations may provide a framework to account for cloud dynamics.

Model results can never be interpreted as conclusive. Ideally, the model employed here will be verified by applying it to specific regions. Soil moisture feedbacks may be more easily testable than vegetation cover feedbacks, as the latter may not vary much in observed history. As mentioned in the introduction, verifying the existence of feedbacks using purely empirical approaches is challenging at best. Granger causality has been used as a statistical tool to detect a causal influence of soil moisture on precipitation [*Salvucci et al.*, 2002; *Notaro*, 2008]. However, even positive Granger causality results cannot be unambiguously related to the existence of a soil moisture-precipitation feedback. Since evapotranspiration and gravitational drainage cause soil moisture to decrease with time after a rainstorm, it has a strong negative auto-

correlation. The combination of soil moisture's auto-correlation and auto-correlation in the precipitation record [*Katz and Parlange, 1995*] may result in the appearance of a negative feedback between soil moisture and precipitation even when there is no physical feedback mechanism [*Salvucci et al., 2002; Wei et al., 2008*]. Empirical verification of soil moisture-precipitation feedbacks thus needs to include testing of several intermediate variables, such as near-surface humidity.

4.2.2 Patterned vegetation

Like precipitation feedbacks, the timescales of vegetation pattern shift determined in Chapter 3 must also be verified empirically. To do so, vegetation pattern and precipitation observations must be available concurrently. Because of the high spatial variability of rainfall in the Sahel, this likely requires ground-based observations. Furthermore, state-of-the-art spatial vegetation pattern models, including the one used in this thesis, were designed primarily phenomenologically, i.e. with a focus on building a simple model that replicates patterned behavior, rather than on capturing all the underlying physical processes and making predictions that are as accurate as possible. As a result of their relative simplicity, they were also not designed to run on the short timescales necessary to force the atmospheric boundary layer model used here. Additional fieldwork is needed before models that correctly represent the biogeophysical processes underlying vegetation patterning can be build. A dedicated field station is probably required. Although setting up such a field station may be costly, it is necessary in order to progress on understanding the relationship between vegetation patterns and desertification. Measurements are needed to improved understanding of several factors contributing to the formation of vegetation patterns that are currently not sufficiently well-understood. Potential future studies on each of these factors are described below.

4.2.2.1 *Vegetation characteristics*

In many vegetation pattern models, the spread of vegetation is modeled as a diffusive process. As such, it depends solely on the spatial gradients of biomass, which is unrealistic. *Thompson et al.* [2008] replaced the diffusive representation for biomass spread in a pattern model with a more physically based dispersal kernel independent of biomass gradients, resulting in decreases smoothness of the simulated patterns. This improved the comparison between the power spectra of observed and modeled patterns, relative to a diffusive biomass spread model. Additional pattern models exist that are based on competition for space at the individual plant scale [e.g. *Lefever and Lejeune*, 1997]. Whatever the theoretical approach, the parameters used in each of these approaches have so far been lacked a compelling source. Fieldwork is therefore necessary to constrain their values. Several other species-specific values should be measured, such as maximum stomatal conductance, seed dispersal behavior, and the amount of shading provided by biomass.

4.2.2.2 *Surface water dynamics and infiltration*

Some theoretical work has been done to study the degree of inaccuracy of a diffusive overland flow representation [*Thompson et al.*, 2011], as is commonly included in current vegetation pattern models. Such a representation was found to be reasonable if infiltration is dependent on the depth of surface water above it (as typically assumed in pattern models), but not if infiltration is independent of this depth (as in many ‘classical’ infiltration models). Which of these representations is most realistic depends on soil properties, including the presence of macropores, and has to be determined from field observations. The theoretical work of [*Thompson et al.*, 2011] also suggests that the total infiltration subsidy (i.e. the amount of additional water that infiltrates over vegetation sites, relative to what would infiltrate in the absence of overland flow and the accompanying spatial redistribution of surface water) is far

smaller than predicted by classical vegetation pattern models. If overland flow cannot account for the observed [Galle *et al.*, 1999] redistribution of water, belowground mechanisms must also be active.

4.2.2.3 *Belowground redistribution of water*

In current spatial vegetation models, redistribution of belowground water (soil moisture) occurs through a diffusive process that counteracts gradients imposed by increased water uptake below vegetation cover. Several models also include a feedback between biomass and root extent, whereby more extensive root networks develop under increased biomass to support the increased water needs [e.g. Lefever and Lejeune, 1997; Gilad *et al.*, 2007]. It is not clear how much each of these processes contributes to the total redistribution of belowground water. Extensive lateral root networks have been observed in Niger [Barbier *et al.*, 2008]. Barbier *et al.* [2008] also found that while there was little to no variation in soil moisture between vegetated and bare soil areas shortly after rainfall, soil moisture decreases faster after a rain storm in bare soil areas than in vegetated patches. The authors interpret this as indicative of reduced soil evaporation over vegetated patches due to increased shading [von Hardenberg *et al.*, 2001]. However, it is not clear whether this shading feedback can necessarily offset transpiration of vegetation, and whether the difference in decay rates can be attributed entirely to changes in evapotranspiration. The sustained increased decay rates below bare soil indicates diffusive mechanisms cannot be solely responsible for belowground water redistribution. Additional field observations of root extent and soil moisture in a variety of patterned vegetation sites are needed to determine whether the results of Barbier *et al.* [2008] are representative, and to what degree relationships between vegetation and lateral root growth might vary between different species that can form patterned vegetation. It may also be instructive to study the relationship between biomass and root growth under different levels of

water availability in the laboratory, particularly in the context of determining how root extent responds to gradual desertification and the accompanying reduction in vegetation cover. Timescales of root decay may impose additional hysteresis when belowground water is redistributed primarily through large lateral root networks. Additionally, a model-based study conceptually similar to that of *Thompson et al.* [2008] can be performed. The effect of including a root augmentation feedback on the energetic modes of the resulting vegetation simulations should be studied.

4.2.2.4 *Atmospheric boundary layer development*

The results of Chapter 3 indicate that atmospheric boundary layer development must be accounted for in order to move from understanding patterns to using them in a quantitative and predictive fashion to inform management decisions. The radiosonde observations used in Chapter 3 were taken at the Niamey airport in Niger. Ideally, radiosonde observations should be taken for at least a full year at a location where vegetation patterns are observed. Such observations incorporate the surface conditions appropriate for studies of vegetation patterning, and can be used to verify the model of Chapter 3 (or an improved version of it). When patterns in other parts of the globe are studied, appropriate radiosonde observations must be used. Lastly, field measurements of the contrast in albedo between vegetated and bare soil patches are necessary. This contrast controls the size of the radiative feedback discussed in Chapter 3, a significant part of the total vegetation pattern-precipitation feedback.

4.3 Broader implications

By coupling a model of land surface conditions to a rainfall model to study the effect of feedbacks, the system under consideration increased. That is, what were traditionally considered boundary conditions (e.g. rainfall) is now a part of the dynamic system. It is potentially informative to increase the system boundaries

even further, to the earth system as a whole. In the earth system, solar radiation provides the only remaining boundary flux between the system and the rest of the universe, and can be considered essentially constant. The study of such a large, closed system invites a thermodynamic approach. A thermodynamic approach may also be useful for elucidating why spatial vegetation patterns continue to exist when the second law of thermodynamics would be expected to homogenize the system. Similarly, the temporal and spatial intermittency of precipitation is surprising, given that this intermittency provides a limit to behavior that is otherwise self-similar. The principle of maximum entropy production (MEP) offers one possible solution. The MEP asserts that far from equilibrium, systems will operate in such a way that the *rate* of entropy production is maximized. The MEP does not postulate a scale over which maximization occurs, which causes ambiguities in its applications [Volk and Pauluis, 2010]. A full discussion of the merits and flaws of MEPs and other global optimality theories is well beyond the scope of this thesis. Nevertheless, a thermodynamic approach to studying hydrology may well be informative and has not been widely considered. Work on a thermodynamic theory of the hydrologic cycle has begun.

Appendix A

Model equations

A summary of model equations and parameters is presented here. Reference sources for the various equations are given in the text of Chapter 2. The full model is run each day from sunrise to sunset, with a timestep of two minutes (reducing the timestep further does not change the results). At each timestep, the system is checked for rainfall ‘triggering’.

A.1 Soil moisture

Soil moisture s is modeled using a standard bucket model,

$$nZ_r \frac{ds}{dt} = P - \frac{\lambda E}{\rho \lambda} - L_d. \quad (\text{A.1})$$

where n (here 0.45) is the soil porosity, Z_r is the rooting depth (here 0.3 m), P is the precipitation intensity, λE is the latent heat flux, ρ is the density of air, λ is the latent heat of vaporization of water, and L_d is the drainage. L_d is modeled according to a Darcian flux assuming a unit gradient at depth $z = Z_r$, $L_d = K(s)$. The hydraulic

conductivity $K(s)$ is modeled according to [Clapp and Hornberger, 1978], given as

$$K(s) = K_{sat}s^{2b+3} \quad (\text{A.2})$$

Parameter values for saturated hydraulic conductivity K_{sat} and b are those for a loamy soil: $K_{sat} = 6.95 \times 10^{-6} \text{ m s}^{-1}$ and $b=5.39$.

A.2 Surface energy partitioning

A one-dimensional energy balance is used at the surface,

$$R_n = \lambda E + H + G \quad (\text{A.3})$$

where the ground heat flux G is parameterized according to

$$G = 0.15R_n. \quad (\text{A.4})$$

We then define Q_n as the available energy flux,

$$Q_n = H + \lambda E = 0.85R_n. \quad (\text{A.5})$$

The net radiation is modeled using an astronomical equation for shortwave radiation

$$R_n = \frac{W_0}{r^2} \cos \beta \quad (\text{A.6})$$

where $W_0 = 1353 \text{ W m}^{-2}$ is the solar constant, r is a correction for the Earth's distance from the sun that varies depending on the day of year D (here 170), and β is the zenith angle.

$$r = 1.0 + 0.017 \cos \frac{2\pi}{365} (186 - D) \quad (\text{A.7})$$

$$\cos \beta = \cos \varphi \cos h_a \cos \delta + \sin \phi \sin \delta, \quad (\text{A.8})$$

where φ is the latitude (34° in Chapter 2, and 15° in Chapter 3), h_a is the hour angle and δ is the solar declension. To be able to study the effects of the magnitude of

R_n , R_n is rescaled at each timestep such that the maximum R_n equals the control parameter R_n^{\max} .

λE is modeled using the Penman-Monteith equation,

$$\lambda E = \frac{\Delta Q_n + \rho c_p VPD g_a}{\Delta + \gamma(1 + \frac{g_a}{g_s})} \quad (\text{A.9})$$

where Δ is the slope of saturated vapor pressure with respect to temperature and γ is the psychrometric constant. The aerodynamic conductance g_a is assumed constant at $\frac{1}{75}$ m s⁻¹. Stomatal conductance g_s is modeled using the Jarvis formulation [Jarvis, 1976], such that

$$g_s = g_{\max} f_1(S) f_2(T) f_3(VPD) f_4(s). \quad (\text{A.10})$$

The incident sunlight S is taken to be equivalent to R_n , such that

$$f_1(S) = \frac{R_n(1 + c/1000)}{c + R_n}, \quad (\text{A.11})$$

where the parameter c has a value of 100.

$$f_2(T) = 1 - k(T - T_{opt})^2, \quad (\text{A.12})$$

where $k=0.16$ and $T_{opt}=298$ K.

$$f_3(VPD) = 1 - m \log VPD, \quad (\text{A.13})$$

where $m=0.6$.

$$f_4(s) = \begin{cases} 0 & \text{if } s \leq s_w \\ \frac{s-s_w}{s^*-s_w} & \text{if } s_w \leq s \leq s^* \\ 1 & \text{if } s > s^* \end{cases} \quad (\text{A.14})$$

where the soil wilting point $s_w = 0.2$ and the critical value of soil moisture $s^* = 0.35$.

Once λE is known, the sensible heat flux H can be simply determined by rearranging the energy balance

$$H = 0.85R_n - \lambda E \quad (\text{A.15})$$

A.3 Atmospheric boundary layer growth

The diurnal evolution of the boundary layer height h is given by

$$\frac{dh}{dt} = \frac{(1 + 2A)\overline{(\theta'\omega')_s}}{\gamma_\theta h} \quad (\text{A.16})$$

where γ_θ is the lapse rate of the free atmospheric potential temperature profile, and A is the entrainment parameter after [Tennekes, 1973]. $A = \frac{\overline{(\theta'\omega')_h}}{\overline{(\theta'\omega')_s}}$ is the ratio of the entrainment flux at h to the surface flux of θ , and has a value of 0.2 here. $\overline{(\theta'\omega')_s} = \frac{H}{\rho c_p}$, where ρ is the air density and c_p is the specific heat capacity of dry air at constant pressure.

Mixed layer temperature and humidity are determined using conservation equations for a slab model

$$h \frac{d\theta}{dt} = \frac{H}{\rho c_p} + (\theta_f - \theta) \frac{dh}{dt} \quad (\text{A.17})$$

$$h \frac{dq}{dt} = \frac{E}{\rho \lambda} + (q_f - q) \frac{dh}{dt} \quad (\text{A.18})$$

where θ_f and q_f are the potential temperature and humidity in the FA at height above the surface h .

A.4 Rainfall depth

Rainfall is only ‘triggered’ if h crosses the lifting condensation level, and if $-z/L > 5$. Here, L is the Obukhov length, given as

$$L = \frac{-u_*^3 \theta}{\kappa_v g w' \theta'} \quad (\text{A.19})$$

Above, u_* is the friction velocity, $\kappa_v = 0.41$ is von Karman’s constant, and g is gravitational acceleration. The diurnal cycle of the friction velocity is prescribed

based on observed values at the Duke Forest, ensemble-averaged each half hour over 8 years of summertime data. The precipitation amount P is given by

$$P = 0.7 \int_0^{2h} q(t_0) dz \quad (\text{A.20})$$

Above, h is the boundary layer height at the time of rainfall initiation t_0 and z is the height above the surface

Bibliography

- Andre, J. C., J. P. Goutorbe, and A. Perrier (1986), HAPEX-MOBILY - a hydrologic atmospheric experiment for the study of water-budget and evaporation flux at the climatic scale, *B. Am. Meteorol. Soc.*, *67*, 138–144.
- Avissar, R., and T. Schmidt (1997), An evaluation of the scale at which ground-surface heat flux patchiness affects the convective boundary layer using a large-eddy simulation model, *J. Atmos. Sci.*, *55*, 2666–2689.
- Baidya Roy, S., and R. Avissar (2002), Impact of land use/land cover change on regional hydrometeorology in Amazonia, *J. Geophys. Res. - Atmos.*, *107*, 8037.
- Baidya Roy, S., G. C. Hurtt, C. P. Weaver, and S. W. Pacala (2003a), Impact of historical land cover change on the July climate of the United States, *J. Geophys. Res. - Atmos.*, *108*, 4793.
- Baidya Roy, S., C. P. Weaver, D. S. Nolan, and R. Avissar (2003b), A preferred scale for landscape forced mesoscale circulations?, *J. Geophys. Res. - Atmos.*, *108*, 88,554.
- Barbe, L. L., T. Lebel, and D. Tapsoba (2002), Rainfall variability in West Africa during the years 1950-1990, *J. Clim.*, *15*, 187–202.
- Barbier, N., P. Coutron, J. Lejoly, V. Deblauwe, and O. Lejeune (2006), Self-organized vegetation patterning as a fingerprint of climate and human impact on semi-arid ecosystems, *J. Ecol.*, *94*(3), 537–547, doi:10.1111/j.1365-2745.2006.01126.x.
- Barbier, N., P. Coutron, R. Lefever, V. Deblauwe, and O. Lejeune (2008), Spatial decoupling of facilitation and competition at the origin of gapped vegetation patterns, *Ecology*, *89*, 1521–1531.
- Bierkens, M. F. P., and B. J. J. M. van den Hurk (2007), Groundwater convergence as a possible mechanism for multi-year persistence in rainfall, *Geophys. Res. Letters*, *34*, L02,402, doi:doi:10.1029/2006GL028396.
- Borgogno, F., P. D’Odorico, F. Laio, and L. Ridolfi (2009), Mathematical models of vegetation pattern formation in ecohydrology, *Rev. Geophys.*, *47*, RG1005.

- Breshaers, D. D., et al. (2005), Regional vegetation die-off in response to global-change type drought, *P. Natl. Acad. Sci. USA*, *102*, 15,144–15,148.
- Brovkin, V., M. Claussen, V. Petoukhov, and A. Ganopolski (1998), On the stability of the atmosphere-vegetation system in the Sahara/Sahel region, *J. Geophys. Res.-Atmos.*, *103*(D24), 31,613–31,624.
- Brubaker, K. L., and D. Entekhabi (1995), An analytic approach to modeling land atmosphere interaction. 1. Construct and equilibrium behavior, *Water Resour. Res.*, *31*(3), 619–632.
- Brunsell, N. A. (2006), Characterization of land-surface precipitation feedback regimes with remote sensing, *Remote Sens. Env.*, *100*, 200–211.
- Brutsaert, W. (1975), On a derivable formula for long wave radiation from clear skies, *Water Resour. Res.*, *11*, 743–744.
- Brutsaert, W. (2005), *Hydrology: An Introduction*, Cambridge University Press, Cambridge, 605 pp.
- Charney, J. G. (1975), Dynamics of deserts and drought in the Sahel, *Q. J. Roy. Meteor. Soc.*, *101*, 193–202.
- Clapp, R. B., and G. M. Hornberger (1978), Empirical equations for some soil-hydraulic properties, *Water Resour. Res.*, *14*(4), 601–604.
- Daly, E., A. Porporato, and I. Rodriguez-Iturbe (2004), Coupled dynamics of photosynthesis, transpiration, and soil water balance. part I: Upscaling from hourly to daily level, *J. Hydrometeorol.*, *5*(3), 546–558.
- de Boer, H. J., E. I. Lammertsma, F. Wagner-Cremer, D. L. Dilcher, M. J. Wassen, and S. C. Dekker (2011), Climate forcing due to optimization of maximal leaf conductance in subtropical vegetation under rising CO₂, *P. Natl. Acad. Sci. USA*, *108*, 4041–4046.
- Deblauwe, V., N. Barbier, P. Couteron, O. Lejeune, and J. Bogaert (2008), The global biogeography of semi-arid periodic vegetation patterns, *Global Ecol. Biogeogr.*, *17*(6), 715–723, doi:10.1111/j.1466-8238.2008.00413.x.
- Deblauwe, V., P. Couteron, O. Lejeune, J. Bogaert, and N. Barbier (2011), Environmental modulation of self-organized periodic vegetation patterns in sudan, *Ecography*, *in press*.
- Dekker, S. C., M. Rietkerk, and M. F. P. Bierkens (2007), Coupling microscale vegetation-soil water and macroscale vegetation-precipitation feedbacks in semi-arid ecosystems, *Global Change Biol.*, *13*(3), 671–678, doi:10.1111/j.1365-2486.2007.01327.x.

- Dekker, S. C., H. J. de Boer, V. Brovkin, K. Fraedrich, M. J. Wassen, and M. Rieterkerk (2010), Biogeophysical feedbacks trigger shifts in the modelled vegetation-atmosphere system at multiple scales, *Biogeosciences*, *7*, 1237–1245.
- Dirmeyer, P. A., R. D. Koster, and Z. C. Guo (2006), Do global models properly represent the feedback between land and atmosphere?, *J. Hydrometeorol*, *7*(6), 1177–1198.
- D’Odorico, P., and A. Porporato (2004), Preferential states in soil moisture and climate dynamics, *Proc. Nat. Acad. Sci.*, *101*(24), 8848–8851, doi:10.1073/pnas.0401428101.
- Dunkerley, D. (2000), Hydrologic effects of dryland shrubs: defining the spatial extent of modified soil water uptake rates at an Australian desert site, *J. Arid. Env.*, *45*, 159–172.
- Eagleson, P. S. (1970), *Dynamic Hydrology*, 462 pp., McGraw-Hill, New York.
- Easterling, D., G. A. Meehl, C. Parmesan, S. A. Changnon, T. R. Karl, and L. O. Mearns (2000), Climate extremes: Observations, modeling, and impacts, *Science*, *289*.
- Ek, M. B., and A. A. M. Holtslag (2004), Influence of soil moisture on boundary layer cloud development, *J. Hydrometeorol*, *5*(1), 86–99.
- Entekhabi, D. (1995), Recent advances in land-atmosphere interaction research, *Rev. Geophys.*, *33*, 995–1004.
- Ferguson, I. M., and R. M. Maxwell (2010), Role of groundwater in watershed response and land surface feedbacks under climate change, *Water Resour. Res.*, *46*, W00F02, doi:doi:10.1029/2009WR008616.
- Findell, K. L., and E. A. B. Eltahir (2003), Atmospheric controls on soil moisture-boundary layer interactions. Part I: Framework development, *J. Hydrometeorol*, *4*(3), 552–569.
- Galle, S., M. Ehrmann, and C. Peugeot (1999), Water balance in a banded vegetation pattern - a case study of tiger bush in western Niger, *Catena*, *37*, 197–216.
- Garratt, J. R. (1992), *The Atmospheric Boundary Layer*, 316 pp., Cambridge University Press, Cambridge.
- Gilad, E., J. von Hardenberg, A. Provenzale, M. Schachak, and E. Meron (2007), A mathematical model of plants as ecosystem engineers, *J. Theor. Biol.*, *244*, 680–691.

- Grist, J. P., and S. E. Nicholson (2001), A study of the dynamic factors influencing the rainfall variability in the West African Sahel, *J. Climate*, *14*, 1337–1359.
- Guo, Z. C., et al. (2006), GLACE: The Global Land-Atmosphere Coupling Experiment. Part II: Analysis, *J. Hydrometeorol.*, *7*(4), 611–625.
- Guttal, V., and C. Jayaprakash (2007), Self-organization and productivity in semi-arid ecosystems: Implications of seasonality in rainfall, *J. Theor. Biol.*, *248*(3), 490–500, doi:10.1016/j.jtbi.2007.05.020.
- Held, I., T. L. Delworth, J. Lu, K. L. Findell, and T. R. Knutson (2005), Simulation of Sahel drought in the 20th and 21st centuries, *P. Natl. Acad. Sci. USA*, *102*, 17,891–17,896.
- Hermann, S. M., A. Anyamba, and C. J. Tucker (2005), Recent trends in vegetation dynamics of the African Sahel and their relationship to climate, *Global Environ. Chang.*, *15*, 394–404, doi:10.1016/j.gloenvcha.2005.08.004.
- HilleRisLambers, R., M. Rietkerk, F. van den Bosch, H. H. T. Prins, and H. de Kroon (2001), Vegetation pattern formation in semi-arid grazing systems, *Ecology*, *82*(1), 50–61.
- Jackson, R. B., et al. (2005), Trading water for carbon with biological sequestration, *Science*, *310*, 1944–1947.
- Janssen, R. H. H., M. B. J. Meinders, E. H. van Nes, and M. Scheffer (2008), Microscale vegetation-soil feedback boosts hysteresis in a regional vegetation-climate system, *Glob. Change Biol.*, *14*(5), 1104–1112, doi:10.1111/j.1365-2486.2008.01540.x.
- Jarvis, P. G. (1976), Interpretation of variations in leaf water potential and stomatal conductance found in canopies in field, *Philos. Trans. R. Soc. London [Biol.]*, *273*(927), 593–610.
- Juang, J.-Y., A. Porporato, P. C. Stoy, M. B. Siqueira, A. C. Oishi, M. Detto, H.-S. Kim, and G. G. Katul (2007), Hydrologic and atmospheric controls on initiation of convective precipitation events, *Water Resour. Res.*, *43*, W03421, doi:10.1029/2006WR004954.
- Kader, B. A., and A. M. Yaglom (1990), Mean fields and fluctuation moments in unstably stratified turbulent boundary-layers, *J. Fluid Mech.*, *212*, 637–662.
- Katul, G. G., S. Palmroth, and R. Oren (2009), Leaf stomatal responses to vapour pressure deficit under current and CO₂-enriched atmosphere explained by the economics of gas exchange, *Plant, Cell, Environ.*, *32*, 968–979.

- Katz, R. W., and M. B. Parlange (1995), Generalizations of chain-dependent processes - application to hourly precipitation, *Water Resour. Res.*, *31*, 1331 – 1341.
- Kefi, S., M. Rietkerk, C. L. Alados, Y. Pueyo, V. P. Papanastasis, A. ElAich, and P. C. de Ruiter (2007), Spatial vegetation patterns and imminent desertification in Mediterranean arid ecosystems, *Nature*, *449*, 213–217.
- Kefi, S., M. Rietkerk, and G. G. Katul (2008), Vegetation pattern shift as a result of rising atmospheric CO₂ in arid ecosystems, *Theor. Popul. Biol.*, *74*, 332–344.
- Kim, C. P., and D. Entekhabi (1998), Feedbacks in the land-surface and mixed layer energy budgets, *Boundary Layer Meteorol.*, *88*, 1–21.
- Kletter, A. Y., J. von Hardenberg, E. Meron, and A. Provenzale (2009), Patterned vegetation and rainfall intermittency, *J. Theor. Biol.*, *256*(4), 574–583, doi:10.1016/j.jtbi.2008.10.020.
- Koster, R. D., et al. (2004), Regions of strong coupling between soil moisture and precipitation, *Science*, *305*(5687), 1138–1140.
- Koster, R. D., et al. (2006), GLACE: The Global Land-Atmosphere Coupling Experiment. Part I: Overview, *J. Hydrometeorol.*, *7*(4), 590–610.
- Larcher, W. (2003), *Physiological Plant Ecology: Ecophysiology and Stress Physiology of Functional Groups*, 513 pp., Springer-Verlag, Berlin.
- Lebel, T., J. D. Taupin, and N. D. Amato (1997), Rainfall monitoring during HAPEX-Sahel. 1. General rainfall conditions and climatology, *J. Hydrol.*, *188-189*, 74–96.
- Lefever, R., and O. Lejeune (1997), On the origin of Tiger bush, *Bull. Math. Biol.*, *59*, 263–294.
- Lefever, R., N. barbier, P. Couteron, and O. Lejeune (2009), Deeply gapped vegetation patterns: On crown/root allometry, criticality and desertification, *J. Theor. Biol.*, *261*, 194–209.
- Leprun, J. C. (1999), The influences of ecological factors on tiger bush and dotted bush patterns along a gradient from Mali to northern Burkina Faso, *Catena*, *37*, 25–44.
- Lhomme, J. P. (2001), Stomatal control of transpiration: Examination of the Jarvis-type representation of canopy resistance in relation to humidity, *Water Resour. Res.*, *37*(3), 689–699.
- MacFadyen, W. A. (1950), Vegetation patterns in the semi-desert plains of British Somaliland, *Geogr. Jour.*, *116*, 199–211.

- Muller, C. J., L. E. Back, P. A. O’Gorman, and K. A. Emanuel (2009), A model for the relationship between tropical precipitation and column water vapor, *Geophys. Res. Lett.*, *36*, doi:10.1029/2009gl039667.
- Notaro, M. (2008), Statistical identification of global hot spots in soil moisture feedbacks among IPCC AR4 models, *J. Geophys. Res.-Atmos.*, *113*(D9), doi:10.1029/2007jd009199.
- Ollson, L., L. Eklundh, and J. Ardö (2005), A recent greening of the Sahel - trends, patterns and potential causes, *J. Arid Environ.*, *63*, 556–566, doi:10.1016/j.jaridenv.2005.03.008.
- Oren, R., J. S. Sperry, G. G. Katul, D. E. Pataki, B. E. Ewers, N. Phillips, and K. V. R. Schafer (1999), Survey and synthesis of intra- and interspecific variation in stomatal sensitivity to vapour pressure deficit, *Plant, Cell, Environ.*, *22*(12), 1515–1526.
- Pino, D., J. V. G. de Arellano, and S. W. Kim (2006), Representing sheared convective boundary layer by zeroth- and first-order-jump mixed-layer models: Large-eddy simulation verification, *J. Appl. Meteor.*, *45*(9), 1224–1243.
- Pitman, A. (2003), The evolution of, and revolution in, land surface schemes designed for climate models, *Int. J. Climatol.*, *23*, 479–510.
- Porporato, A. (2009), Atmospheric boundary-layer dynamics with constant Bowen ratio, *Bound.-Lay. Meteorol.*, *132*(2), 227–240, doi:10.1007/s10546-009-9400-8.
- Rietkerk, M., M. C. Boerlijst, F. van Langevelde, R. HilleRisLambers, J. van de Koppel, L. Kumar, H. H. T. Prins, and A. M. de Roos (2002), Self-organization of vegetation in arid ecosystems, *Am. Nat.*, *160*(4), 524–530.
- Rietkerk, M., S. C. Dekker, P. C. de Ruiter, and J. van de Koppel (2004), Self-organized patchiness and catastrophic shifts in ecosystems, *Science*, *305*(5692), 1926–1929.
- Salvucci, G. D., J. A. Saleem, and R. Kaufmann (2002), Investigating soil moisture feedbacks on precipitation with tests of Granger causality, *Adv. Water Resour.*, *25*(8-12), 1305–1312.
- Santanello, J. A., M. A. Friedl, and M. B. Ek (2007), Convective planetary boundary layer interactions with the land surface at diurnal time scales: Diagnostics and feedbacks, *J. Hydrometeorol.*, *8*, 1082–1097, doi:10.1175/jhm614.1.
- Scheffer, M., M. Holmgren, V. Brovkin, and M. Claussen (2005), Synergy between small- and large-scale feedbacks of vegetation on the water cycle, *Glob. Change Biol.*, *11*, 1003–1012.

- Sellers, P., F. Hall, G. Asrar, D. E. Strebel, and R. E. Murphy (1992), An overview of the First International Sattelite Land Surface Climatology Project (ISLSCP) Field Experiment (FIFE), *J. Geophys. Res.*, *97*, 18,345–18,371.
- Shukla, J., and Y. Mintz (1982), Influence of land-surface evapo-transpiration on the earth’s climate, *Science*, *215*, 1498–1501.
- Siqueira, M., G. Katul, and A. Porporato (2009), Soil moisture feedbacks on convection triggers: The role of soil-plant hydrodynamics, *J. Hydrometeorol.*, *10*(1), 96–112, doi:10.1175/2008jhm1027.1.
- Taylor, C. M., and R. J. Ellis (2006), Satellite detection of soil moisture impacts on convection at the mesoscale, *Geophys. Res. Lett.*, *33*, L03,404.
- Tennekes, H. (1973), Model for dynamics of inversion above a convective boundary-layer, *J. Atmos. Sci.*, *30*(4), 558–567.
- Thompson, S., G. Katul, and S. M. McMahon (2008), Role of biomass spread in vegetation pattern formation within arid ecosystems, *Water Resour. Res.*, *44*(10), doi:10.1029/2008wr006916.
- Thompson, S., G. G. Katul, A. G. Konings, and L. Ridolfi (2011), Unsteady overland flow on at surfaces induced by spatial permeability contrasts, *Submitted to Adv. Water. Resour.*
- Ursino, N., and S. Contarini (2006), Stability of banded vegetation patterns under seasonal rainfall and limited soil moisture storage capacity, *Adv. Water Resour.*, *29*(10), 1556–1564, doi:10.1016/j.advwatres.2005.11.006.
- Valentin, C., and J. M. d’Herbes (1999), Niger tiger bush as a natural water harvesting system, *Catena*, *37*(1-2), 231–256.
- van de Koppel, J., et al. (2002), Spatial heterogeneity and irreversible vegetation change in semiarid grazing systems, *Am. Nat.*, *159*(2), 209–218.
- van den Hurk, B., and E. van Meijgaard (2010), Diagnosing land-atmosphere interaction from a regional climate model simulation over West Africa, *J. Hydrometeorol.*, *11*(2), 467–481, doi:10.1175/2009jhm1173.1.
- van Heerwaarden, C. C., J. V. G. de Arellano, A. F. Moene, and A. A. M. Holtslag (2009), Interactions between dry-air entrainment, surface evaporation and convective boundary-layer development, *Q. J. R. Meteorol. Soc.*, *135*(642), 1277–1291, doi:10.1002/qj.431.
- van Heerwaarden, C. C., J. V. G. de Arellano, A. Gounou, F. Guichard, and F. Couvreux (2010), Understanding the daily cycle of evapotranspiration: a method to quantify the influence of forcings and feedbacks, *J. Hydrometeorol.*, *11*, 1405–1422, doi:10.1175/2010JHM1272.1.

- Volk, T., and O. Pauluis (2010), It's not the entropy produce, rather how you produce it, *Philos Trans R Soc London [Biol]*, *365*, 1317–1322.
- von Hardenberg, J., E. Meron, M. Schachak, and Y. Zarmi (2001), Diversity of vegetation patterns and desertification, *Phys. Rev. Lett.*, *87*, 198,101.
- Wang, G. L., and E. A. B. Eltahir (2000a), Ecosystem dynamics and the Sahel drought, *Geophys. Res. Lett.*, *27*, 795–798.
- Wang, G. L., and E. A. B. Eltahir (2000b), Role of vegetation dynamics in enhancing the low-frequency variability of the Sahel rainfall, *Water Resour. Res.*, *36*, 1013–1021.
- Wang, J., F. J. F. Chagnon, E. R. Williams, A. K. Betts, N. O. Renno, L. A. T. Machado, G. Bisht, R. Knox, and R. L. Bras (2009), Impact of deforestation in the Amazon basin on cloud climatology, *P. Natl. Acad. Sci. USA*, *106*, 3670–3674.
- Wei, J. F., R. E. Dickinson, and H. S. Chen (2008), A negative soil moisture-precipitation relationship and its causes, *J. Hydrometeor.*, *9*(6), 1364–1376, doi:10.1175/2008jhm955.1.
- Werth, D., and R. Avissar (2002), The local and global effects of Amazon deforestation, *J. Geophys. Res. - Atmos.*, *107*, 8087.
- Wu, C. M., B. Stevens, and A. Arakawa (2009), What controls the transition from shallow to deep convection?, *J. Atmos. Sci.*, *66*(6), 1793–1806, doi:10.1175/2008jas2945.1.
- Zeng, N. (2003), Drought in the Sahel, *Science*, *302*, 999–1000.
- Zeng, N., J. D. N. nd K.-M. Lau, and C. J. Tucker (1999), Enhancement of inter-decadal climate variability in the Sahel by vegetation interaction, *Science*, *286*, 1537–1540.